Heat waves monitoring over West African cities: uncertainties, characterization and recent trends

Cedric G. Ngoungue Langue[1,2], Christophe Lavaysse[2,3], Mathieu Vrac[4], and Cyrille Flamant[1]

[1]Laboratoire Atmosphères, Milieux, Observations Spatiales (LATMOS) - UMR 8190 CNRS/Sorbonne Université/UVSQ, 78280 Guyancourt, France.
[2]Université Grenoble Alpes, CNRS, IRD, G-INP, IGE,38000 Grenoble, France
[3]European Commission, Joint Research Centre (JRC), 21027 Ispra, VA, Italy
[4]Laboratoire des Sciences du Climat et de l'Environnement, CEA Saclay l'Orme des Merisiers, UMR 8212 CEA-CNRS-UVSQ, Université Paris-Saclay & IPSL, 91191 Gif-sur-Yvette, France.

Correspondence: Ngoungue Langue Cedric Gacial (cedric-gacial.ngoungue-langue@latmos.ipsl.fr)

Abstract.

Heat waves can be one of the most dangerous climatic hazards affecting the planet; having dramatic impacts on the health of humans and natural ecosystems as well as on anthropogenic activities, infrastructures and economy. Based on climatic conditions in West Africa, the urban centers of the region appear to be vulnerable to heat waves. The goals of this work is firstly to assess the potential uncertainties encountered in heat waves detection; and secondly analyse their recent trend in West Africa cities during the period 1993-2020. This is done using two state-of-the-art reanalysis products, namely ERA5 and MERRA, as well as two local station datasets, namely Yoff Dakar in Senegal and Aéroport Félix Houphouët Boigny Abidjan in Ivory Coast. An estimate of station data from reanalyses is processed using an interpolation technique : the nearest neighbor to the station with a land sea mask >=0.5; the interpolated temperatures from local station in Dakar and Abidjan, show slightly better correlation with ERA5 than MERRA. Three types of uncertainties are discussed: the first type of uncertainty is related to the reanalyses themselves, the second is related to the sensitivity of heat waves frequency and duration to the threshold values used to monitor them; and the last one is linked to the choice of indicators and the methodology used to define heat waves. Three sorts of heat waves have been analysed, namely those occurring during daytime, nighttime and both daytime and nighttime concomitantly. Four indicators have been used to analyse heat waves based on 2-m temperature, humidity, 10-m wind or a combination of these. We found that humidity plays an important role in nighttime events; concomitant events detected with wet-bulb temperature are more frequent and located over the north Sahel. For all indicators, we identified 6 years with a significantly higher frequency of events (1998, 2005, 2010, 2016, 2019 and 2020) possibly due to higher sea surface temperatures in the equatorial Atlantic ocean corresponding to El Nino events for some years. A significant increase in the frequency, duration and intensity of heat waves in the cities has been observed during the last decade(2012-2020); this is thought to be a consequence of climate change acting on extreme events.

Keywords : heat extremes, El Niño, reanalysis data, climate change, climatic regions, West Africa.

1 Introduction

Since the industrial revolution, the Earth is experiencing a global warming related to human activity ((Hartmann et al., 2013); Intergovernmental Panel on Climate Change-IPCC-report 2021). The last report of IPCC shows that this warming will exceed $1.5°C$ with respect to the IPCC baseline 1850-1900 under different Shared Socio-economic Pathways (SSP) in 2100 if the rate of greenhouse gas emissions is not reduced. This warming climate contributes to the occurrence of extreme events, but also tends to reinforce their intensity ((Fischer and Schär, 2010; Engdaw et al., 2022); IPCC report, 2021). Heat waves appear as one of the most dangerous climatic hazards affecting the planet due to their impacts on several sectors (Perkins, 2015). The health sector is the most affected; heat waves act on the thermal comfort of the body leading to an increase in morbidity, respiratory and cardiovascular diseases among the most vulnerable population (children and eldery) (e.g., Huynen et al., 2001; Braga et al., 2002; Hajat et al., 2007; Kovats and Hajat, 2008; Anderson and Bell, 2009; Gasparrini and Armstrong, 2011; Rocklöv et al., 2014). Heat waves are "silent killers" because their impacts on human health are not usually instantaneous (Loughnan, 2014). In 2003, an intense heat wave occurred in France, killing more than 14000 people (Fouillet et al., 2006). During this event, temperatures sometimes reached 37°C, a record since 1950. This event was very persistent and lasted two weeks in France. In addition to this event, the Russian heat wave in 2010 caused numerous destruction (dysfunction of railway stations, interruption of energy production) and more than 11000 deaths (Shaposhnikov et al., 2014). Temperature sometimes reached 38°C and generated huge fires in the neighboring regions of Moscow; and a high concentration of carbon monoxide in the troposphere. In April 2010, northern Africa was affected by a severe heat wave with daily maximum temperatures frequently exceeding 40°C and daily minimum temperatures over 27°C for more than five consecutive days (Largeron et al., 2020).

Heat waves are natural disasters often associated with an increase in daytime and/or nighttime temperatures. More generally, they are defined as a period of consecutive days for which the temperatures are much hotter than the normal. There is no universal formulation describing a heat wave, however a definition could be made according to the context of the study (health, environment, infrastructure, agriculture, energy supply). From a physiological point of view, the severity of a heat wave is measured through its duration and intensity.

West Africa experiences a very hot and dry climate over the Sahel region, and a hot and humid climate over the Guinea coast. The climatic conditions over West Africa make the region vulnerable to heat waves when it comes to the health of humans and natural ecosystems, but also agriculture. Many studies on heat waves have been carried out in Europe. However, heat waves in Africa are still not well documented. Moron et al. (2016) analyzed the trends of extreme temperatures in the northern tropical Africa from observations and reconstructed data. They show that heat waves indices over the region were highly correlated with the El Niño-southern Oscillation indices (ENSO). Barbier et al. (2018) investigated the intraseasonal variability of large-scale heat waves during the spring using the Berkeley Earth Surface Temperature (BEST) gridded dataset and reanalyses: the European Centre for Medium-Range Weather Forecasts interim reanalysis (ERA-Interim), Modern-Era Retrospective analysis for Research and Applications (MERRA, see section Data for more details) and the National Centers for Environmental Prediction reanalysis (NCEP-2). They defined heat waves using anomalies of minimum/maximum values of

the 2-m temperature. They found some discrepancies in the characteristics, variability and climatic trends of heat waves in the different products. Largeron et al. (2020) analysed the April 2010 heat wave in North Africa using both the BEST dataset and climate simulations from the atmospheric component of the Centre National de Recherches Météorologiques (CNRM) climate model. They showed a strong link between heat waves over the Sahara and the incoming heat surface fluxes. Another important result of this work, is the radiative effect of water vapor on minimum temperatures during the heat wave period. This can lead to extreme heat conditions during the night and cause death to eldery. Guigma et al. (2020) analysed the characteristics and thermodynamics of Sahelian heat waves using different thermal indices based on temperature, wind speed, relative humidity derived from ERA5 reanalysis (see section Data for more details). They found that most regions in the Sahel suffer on average one or two heat waves per year with a duration of 3-5 days with severe magnitude. They have also shown that the eastern Sahel experienced more frequent and longer events. They identified heat advection and greenhouse effect of moisture as the main drivers of Sahelian heat waves. Some of the previous studies conducted over the Sahelian band, only use the daily maximum and minimum temperatures (e.g. , Moron et al., 2016; Barbier et al., 2018) for the detection of heat waves, thereby ignoring the potential influence of humidity and wind speed. Others take into account the effect of humidity in the heat wave definition (e.g. , Guigma et al., 2020), but information about the interannual and seasonal variability of events detected are missing; even though this is very important for policy makers and governments to take into account in order to develop early alert systems. Recently, Engdaw et al. (2022) studied the trends of heat waves over Africa during the period 1980-2018 using observations from the Climate Research Unit version 4.03 (CRU TS4.03) and BEST datasets as well as the following reanalysis datasets: ERA5, MERRA-2 and the Japanese Meteorological Agency's 55-year reanalysis (JRA-55). They highlighted large differences in both trend and temporal evolution of heat wave indices between the different reanalyses. They found a peak of heat over northern and western Africa in 2010 as well as in 2016 over eastern and southern Africa. They noticed a significant warming and an increase in heat wave occurrence in all the regions in Africa. However, Engdaw et al. (2022) focused only on dry heat waves over a large domain of west Africa [20°W-20°E,10°S-15°N]; the duration of heat waves were not addressed, nor the evolution of wet heat waves.

The most lethal heat waves are not only due to high temperature, but also to the effect of humidity (Steadman, 1979a, b); hot and humid conditions (as is the case in coastal regions) can be more dangerous than equivalently hot but dry conditions (Wehner et al., 2017). Wet heat waves, which are the most dangerous for human health, were not investigated in the previous works. Following Steadman (1979a, b), one can legitimately wonder about the effect of humidity on the frequency of heat waves and on the evolution of humid heat waves in west African cities. Based on previous studies, different definitions of heat wave have been proposed leading to differences in results. This is because there is no universal definition of a heat wave; based on the research applications, some indicators and definitions can be adopted. Thereby, we can wonder about the potential sources of uncertainty found in the analysis of heat waves.

The goals of this paper are: (i) to highlight the potential uncertainties encountered in the heat wave detection process, and (ii) to analyse the recent trend and characteristics of dry and wet heat waves over a selection of West African cities grouped in

climatic regions. To reach these aims, we firstly evaluate the biases in the reanalyses (ERA5 and MERRA) using ERA5 as the reference; secondly the sensitivity of heat wave occurrence respectively to the threshold values, indicators and methods applied to define heat waves are investigated. Finally, we assess the temporal variability (seasonal and interannual) of heat waves and their characteristics in different climatic regions over West Africa.

The remainder of this article is organised as follows: in section 2, we present the regions of interest and the data used for this work; the description of the methodology is also provided. Section 3 contains the main results of this study following the methodology described in section 2. In section 4, the uncertainty in the reanalyses and the origin of coastal heat waves are discussed. Section 5 provides a conclusion and some perspectives for future works.

2   Region of interest, Data and Methods

2.1   Region of interest

The current study is conducted over west Africa which is located over a domain [5-20°N, 15°W-10°E], and spans from the Atlantic coast to Chad, and from the Gulf of Guinea to the southern fringes of the Sahara desert [Fig1]. The climate in west Africa is mostly influenced by the West African monsoon flux which governs the rainy season and thus the rain-fed agriculture. The West Africa region has a semi-arid and hot climate with a dry season (Koppen classification BSh or BShw). This climate corresponds to an alternation between a short wet season and a very long dry season. The West Africa region shows high climate variability at regional- and local- scale. In this study, we are interested in the coastal and continental parts of West Africa, therefore, we identified three regions based on their location and their climate variability on which we conducted our analyses. The choice of these regions is coherent with Moron et al. (2016) who used a hierarchical clustering approach to define some blocs of cities over West Africa. The fifteen cities investigated here have been classified in three regions as follows:

– Continental zone (**CONT** hereafter) including the cities of Bamako, Ouagadougou and Niamey [Fig1];

– Coastal atlantic zone (**ATL** hereafter) including the cities of Dakar, Nouakchott, Monrovia and Conakry [Fig1];

– Coastal Guinean zone (**GU** hereafter) including the cities of Yamoussoukro, Abidjan, Lomé, Abuja, Lagos, Accra, Cotonou and Douala [Fig1].

The CONT and GU regions are very similar to the clusters found by Moron et al. (2016) (see figure under the title 'Clusters membership' in Moron et al. (2016)). The ATL region is a specific case because all the cities belonging to the region are not present in the clusters defined by Moron et al. (2016). Therefore, we have investigated the spatial variability of heat wave characteristics for each city. As result, we found coherent evolution between the cities (see [FigS1] in supplement material for maximum values of T2m using the 90th percentile as threshold); and we put them together to form the ATL bloc.

4

2.2 Data

Reanalysis products are often taken as an alternative solution to observational weather and climate data due to availability and accessibility problems, particularly in data-sparse regions such as Africa (Gleixner et al., 2020). In this work, to access information with a regular spatial grid and a large horizontal coverage, we used two state-of-the-art reanalysis products: the fifth-generation European Center for Medium-Range Weather Forecasts (ECMWF) reanalysis (ERA5; (Hersbach et al., 2020)); and the Modern-Era Retrospective analysis for Research and Applications, version 2 (MERRA-2; (Gelaro et al., 2017)) from the National Oceanic Atmospheric Administration (NOAA). ERA5 reanalysis has a native spatial resolution of 0.28125 degree ($\sim 31\ km$) with 137 hybrid sigma/pressure levels from the surface up to $80\ km$, yet downloaded data are interpolated to a regular latitude/longitude grid of 0.25° x 0.25°. ERA5 is produced using 4D-Var data assimilation and model forecasts in CY41R2 of the ECMWF Integrated Forecast System (IFS). MERRA reanalysis has a spatial resolution of 0.625°x0.5° with 42 standard pressure levels. MERRA is using an upgraded version of the Goddard Earth Observing System Model, Version 5 (GEOS-5) data assimilation system and the Global Statistical Interpolation (GSI) analysis scheme of Wu et al. (2002).These two reanalyses dataset are assessed through the Climserv database from the Institut Pierre Simon Laplace (IPSL) server. To be consistent in our analyses, we transformed the spatial resolution of MERRA-2 from 0.625°x0.5° to 0.25°x0.25° to match the one of ERA5; this is done using a first order conservative interpolation. We use hourly data covering the period going from 1 January 1993 to 31 December 2020 both for ERA5 and MERRA. Our choice of ERA5 and MERRA-2 to conduct this study is supported by some previous work showing that these two reanalyses are part of the most relevant used in Africa regions (e.g. , Barbier et al., 2018; Ngoungue Langue et al., 2021; Engdaw et al., 2022). As the main objective here is to process heat waves detection, we focus on atmospheric variables at the surface such as 2-meter temperature ($T2m$), 2-meter relative humidity (Rh), 2-meter dew-point temperature, 2-meter specific humidity, 10-meter wind components and water vapor pressure (e) from which wet bulb temperature (Tw) and Apparent Temperature (AT; (McGregor et al., 2015)) have been computed. These atmospheric variables have a significant impact on human thermal comfort (McGregor et al., 2015). Daily minima and maxima values were computed for $T2m, Tw, AT$ and the Universal thermal Comfort Index ($UTCI$; (Di Napoli et al., 2021)). AT is similar to the heat index developed by Steadman (1984). The climate variables e, Tw, AT and Rh were computed using the following formulas:

$$\mathbf{e = 6.1121 * \exp(\frac{17.502 * T}{240.97 + T})} \tag{1}$$

(Buck, 1981; Alduchov and Eskridge, 1996)

$$\mathbf{Tw = T * atan[A(Rh + B)^{\frac{1}{2}}] + atan(T + Rh) - atan(Rh - C) + D * (Rh)^{\frac{3}{2}} * (atan(E * Rh)) - F} \tag{2}$$

(Stull, 2011), (Rh is used in percentage, for example 32 for Rh=32%)

$$145 \quad \mathbf{AT = T + 0.33 * e - 0.70 * W_s - 4.00} \tag{3}$$

(McGregor et al., 2015)

Rh is computed differently based on the variables available in the products. The first formula is used to compute Rh in ERA5, and the second is used for MERRA.

$$\mathbf{Rh = 100 * \frac{\exp(\frac{a * T_d}{b + T_d})}{\exp(\frac{a * T}{b + T})}} \tag{4}$$

150 (August, 1828; Magnus, 1844; Alduchov and Eskridge, 1996)

$$\mathbf{Rh = 0.263 * p * q * [\exp(\frac{17.67 * (T - T_0)}{T - 29.65})]^{-1}} \tag{5}$$

https://earthscience.stackexchange.com/questions/2360/how-do-i-convert-specific-humidity-to-relative-humidity

$\mathbf{a} = 17.625, \mathbf{b} = 243.04, \mathbf{A} = 0.151977, \mathbf{B} = 8.313659, \mathbf{C} = 1.676331, \mathbf{D} = 0.00391838, \mathbf{E} = 0.023101, \mathbf{F} = 4.686035, \mathbf{T_0} = 273.16K$

155 Where $\mathbf{T}$(°C), $\mathbf{T_d}$(°C), $\mathbf{T_0}$(K), $\mathbf{p}$(hPa), $\mathbf{W_s}$(m/s) and $\mathbf{q}$ are respectively the ambient temperature, dew-point temperature, reference temperature, pressure, wind speed and specific humidity.

The land sea mask dataset used in this work has been derived from ERA5 reanalysis; it can be accessed on the Copernicus Data Store (CDS). T2m daily maximum and minimum observations at Dakar-Yoff station in Senegal and Aéroport Félix Houphouët Boigny (FHB) station in Ivory Coast have been used to evaluate our interpolation method. This is because we don't

160 have access to other station datasets in the regions. The data from Dakar-Yoff extend from 1 January 1973 to 31 December 2018 containing almost 16% of missing values; and the data from Aéroport FHB are from 1 January 2005 to 31 December 2017 with 0.35% missing values. These data have been provided by some colleagues at Agence Nationale de l'Aviation Civile et de la Météorologie (ANACIM) for the Dakar-Yoff station, and Institut des Géosciences de l'Environnement (IGE) for the Aéroport FHB station.

165 ## 2.3 Methods

2.3.1 Estimation of atmospheric variables at the scale of cities

Reanalysis dataset used for weather studies are generally run at global scale, therefore information at local scale is missing in many regions; this is a critical issue in regions where there is a lack of observation stations as is the case of African cities. To overcome this problem, sometimes downscaling methods can be used. In this work, we study phenomena at the scale of

the cities and reanalyses (ERA5 and MERRA) have too coarse a spatial resolution. The scales of the reanalyses are more representative of the spatial variability of a heat wave occuring in a city than an isolated local station. Nevertheless, a certain validation must be conducted of testing stations, especially to find the best interpolation technique to estimate local temperature from the reanalyses. This is especially important over the coastal regions. Indeed, most of the cities used in this study are located along the coast and influenced by the ocean air masses (see [Fig1]). The evaluation of the spatial variability of the correlation between the local scale variable (station) and reanalyses (ERA5) for T2m for example, showed high correlation values over the continent [FigS2] (Dakar, Abidjan). This suggests that the station data are well correlated with ERA5 grid points which are located on the continent; so there is a need to know whether a ERA5 grid point is over the continent or not before applying an interpolation technique. To estimate the proportion of land on a grid point, we used the land sea mask (lsm) whose values range from 0 to 1. The land sea mask is a measure of the land occupation on a grid point. A lsm of 0 means no land (a grid point located in the ocean), and a lsm of 1 means that the model cell is fully covered by land. Therefore, to estimate the climate variables over the cities from reanalyses, we use the nearest grid point of reanalyses to the station which satisfies a lsm equal or greater than 0.5 (see [Table1] for lsm values of all the cities considered in this study). This approach was chosen after evaluated different methods such as (see [FigS3a] for more details) :

- a bilinear interpolation using the four nearest grid points of reanalyses around the station [FigS3a (a,d)];

- a linear gradient approach which considers that the gradient of temperature is constant between two grid points based on a linear interpolation with a condition on the lsm value (>=0.5) [FigS3a (c,f)];

- the selection of the nearest grid point of reanalyses from the station with different values of lsm (>=0.5, 0.75 and 1; we only show for lsm>=0.5) [FigS3a (b,e)].

- a dynamical interpolation approach taking into account the effect of winds (not shown).

The interpolation method was applied to ERA5 and MERRA, and the resulting estimated data were compared to the station data by correlation analysis. We found that ERA5 appears to be slightly better than MERRA at both stations (Dakar and Abidjan) for minimum and maximum $T2m$ values [FigS3b].

2.3.2 Heat wave detection

Heat waves are usually defined as consecutive days of extremely hot temperatures above a threshold value of temperature (e.g., Tan et al., 2010; Gasparrini and Armstrong, 2011; Perkins and Alexander, 2013; Wang et al., 2019). Many factors can affect the definition of a heat wave, including the end-user sectors (human health, infrastructures, transport, agriculture) and also the climatic conditions of the regions (Perkins and Alexander, 2013). Therefore, there is no universal and standard definition of a heat wave (Perkins, 2015; Oueslati et al., 2017; Shafiei Shiva et al., 2019). Different thresholds, duration and indicators contribute to divergence in defining heat waves (Smith et al., 2013). Heat waves can be defined from daily meteorological variables such as daily raw temperature (T_{min}, T_{mean} and T_{max}) (e.g., Fontaine et al., 2013; Beniston et al., 2017; Ceccherini et al., 2017; Déqué et al., 2017; Batté et al., 2018; Barbier et al., 2018; Lavaysse et al., 2018; Engdaw et al., 2022), mean daily

wet bulb temperature (Yu et al., 2021) or heat stress indices (e.g., Robinson, 2001; Fischer and Schär, 2010; Perkins et al., 2012a; Guigma et al., 2020) using relative or absolute thresholds. The use of absolute thresholds is well suited to detect heat waves during the year in regions where the seasonal cycle is well marked. In mid-latitudes for example, the seasonal thermal amplitude of $T2m$ is large, approximately 20°C. In tropical regions this method is not suitable since the seasonal thermal amplitude is strongly reduced (6°C). Therefore a relative threshold for heat waves detection is adopted in our study as our region of interest is West Africa. Some authors use the daily anomalies of temperature to define heat waves (e.g., Stefanon et al., 2012; Barbier et al., 2018). Most of the previous studies are focused on daytime or nighttime heat waves, ignoring events which occur during the day and night concomitantly. These type of heat waves are very dangerous for human health because the body suffers from heat stress during the day and night (Lavaysse et al., 2018). In our case, we defined 3 methods to detect specific type of heat waves (namely those occurring during daytime, nighttime and both daytime and nighttime concomitantly) using the daily min and max values of: $T2m$ ($T2m_{min}, T2m_{max}$), Tw (Tw_{min}, Tw_{max}), AT (AT_{min}, AT_{max}) and $UTCI$ ($UTCI_{min}, UTCI_{max}$) as indicators. The selected atmospheric variables have been used for heat wave detection in previous studies; they take in account some key parameters (air temperature, wind, humidity, radiant temperature) to assess the body heat stress and they are easy to compute. The methods applied are defined below :

– **Method 1:** A heat wave is defined as a consecutive period of at least 3 days where daily max value of an indicator exceeds the calendar 90th percentile of daily max values of the indicator computed over the entire period (see **HW1** in [Fig**2**]). This approach is useful for monitoring daytime heat wave events. Daytime events will be more associated with the incoming solar radiation;

– **Method 2:** A heat wave is defined as a consecutive period of at least 3 days where daily min value of an indicator exceeds the calendar 90th percentile of daily min values of the indicator computed over the entire period (see **HW2** in [Fig**2**]). This approach is useful for monitoring nighttime heat wave events. Nighttime events can be related to humidity content in the region;

– **Method 3:** A heat wave is defined as a consecutive period of at least 3 days where daily min and max values of an indicator exceed the calendar 90th percentiles of daily min and max values respectively (see **HW3** in [Fig**2**]). This method is more appropriate for extreme events that happen both during the day and the night and are very harmful for human health.

The 90th percentile is computed for each calendar day of the year using a moving window of 11 days centered on the studied day. Using a moving window, we take into account the seasonal cycle in the computation of percentiles. The use of a relative threshold is more appropriate because it can be easily reproducible in other regions. When two heat wave events are separated by one day characterized by a value of indicator below the daily 90th percentile, they are pooled together to form a single event (see [Fig**2**]).

2.3.3 Heat wave characteristics

Once a heat wave is detected, some key characteristics are derived, namely duration and intensity. Some studies use the Heat Wave Magnitude Index daily (HWMId) to assess the severity of heat waves (e.g., Russo et al., 2016; Ceccherini et al., 2017). The HWMId focuses on strong heat wave events; using this metric, one cannot access the total intensity of all the events detected. In our study, the methodology applied to compute the duration and intensity of heat waves has been developed by Lavaysse et al. (2018) for the monitoring of temperature extremes over Europe. We define the heat wave duration as the total number of hot days in heat waves. Hot days are days in heat waves with daily values of the indicators above the daily thresholds. The heat wave duration is computed using the following expression:

$$\mathbf{duration} = \sum_{i=1}^{N} \sum_{j}^{d} \delta_j \tag{6}$$

where $\delta_j = 1$ if $T_j >$ daily 90th percentile and $\delta_j = 0$ if $T_j <$ daily 90th percentile, N represents the total number of heat waves per grid point and d the number of hot days in a heat wave. The kronecker δ_j is used here because we pooled heat waves separated by 1 day together to form single events. For example, two heat waves with respective duration of 4 and 3 days separated by 1 day below the threshold will be counted as 1 event with a duration of 7 days. For each bloc defined previously, the duration of heat waves is computed as the average of the duration of heat waves over the cities belonging to the same bloc. This apply also for the intensity.

The intensity of a heat wave has been defined as the sum of the daily exceedance of daily values of indicators to the climatological daily threshold in a sequence of hot days. This study is part of the project Agence National de la Recherche STEWARd (STatistical Early WArning systems of weather-related Risks from probabilistic forecasts, over cities in West Africa) project which focuses on climate extremes human impacts. Therefore, the climatological daily threshold is chosen to be constant over the whole period; and it is defined as the minimum of the daily climatology thresholds over the study period. From this approach, we can properly evaluate the severity of a heat wave and its potential human impacts." The expression of the intensity is given by :

$$\mathbf{I_1} = \sum_{t=1}^{T} \mathbf{bool_{max,t,w}} * (\mathbf{X_{max,t,w}} - \min(\mathbf{Q_{max,w}})) \tag{7}$$

$$\mathbf{I_2} = \sum_{t=1}^{T} \mathbf{bool_{min,t,w}} * (\mathbf{X_{min,t,w}} - \min(\mathbf{Q_{min,w}})) \tag{8}$$

$$\mathbf{I_3} = \sum_{t=1}^{T} \mathbf{bool_{min-max,t,w}} * (\mathbf{X_{max,t,w}} - \min(\mathbf{Q_{max,w}})) + \sum_{t=1}^{T} \mathbf{bool_{min-max,t,w}} * (\mathbf{X_{min,t,w}} - \min(\mathbf{Q_{min,w}})) \tag{9}$$

I_1, I_2, I_3 are respectively intensities associated with HW_1, HW_2, HW_3. $X_{max,t,w}, X_{min,t,w}$ are respectively daily max/min values of indicators at the grid point w $Q_{max,w}$, $Q_{min,w}$ represent respectively daily max/min thresholds of the indicators at the grid point w. $bool_{max,t,w}$, $bool_{min,t,w}$ are boolean time series which contain 0 for daily values below the daily thresholds of the indicators, and 1 if daily values are above the daily thresholds respectively. $bool_{min-max,t,w}$ is a boolean time series which indicates 1 if min and max daily values of indicators are above the daily threshold, and 0 if not. T is the length in days of the study period. The mean duration and intensity are used to assess the severity of the heat wave.

2.3.4 Evaluation of the products using statistical metrics (hits rate, ACC, GSS)

Most regions in Africa suffer from a lack of observations due to a small number of meteorological stations available. To access information over a large domain, we use ERA5 and MERRA-2 reanalysis datasets which are very coherent in representing large-scale processes in the Saharan area (Ngoungue Langue et al., 2021). The coherence of reanalyses at regional scale has been evaluated using statistical metrics such as the hits rate, anomaly of correlation (ACC) and the Gilbert skill score (GSS). The hits rate and GSS are used to evaluate hot days in the reanalyses.

– **Hits rate**

The hits rate, also known as the "hit", is a measure of the fraction of events detected in an evaluated dataset knowing that the events happen in the reference at the same time. It is given by the following formula :

$$\text{hit} = \frac{TP}{TP+FP} \tag{10}$$

TP: True positives are events correctly detected by the two datasets at the same time; FP: False positives are events not detected by the evaluated dataset but that occured in the reference. Hit values are ranging from 0 to 1; hit=1 means that all the events observed in the evaluated dataset occurred in the reference.

Some previous work such as (Olauson, 2018; Ramon et al., 2019) found that ERA5 provides a good representation of various near surface meteorological variables including near surface humidity and wind speed in comparison to others reanalyses including MERRA. Therefore for the computation of the hit, we choose ERA5 as the reference and MERRA the evaluated dataset.

– **ACC**

The ACC is similar to a linear correlation, the only difference is that it is computed using the anomalies of variables with respect to the climatology. This metric is stricter than the simple correlation and not sensitive to the seasonal cycle which tends to increase the correlation between the products. ACC takes values between -1 and 1. ACC=1 indicates a perfect correlation between the products. For example, to compute the ACC between ERA5 and MERRA using the variable T2m in this study, we firstly compute the anomalies between each reanalysis and their respective climatologies; secondly we compute the correlation between the resulting anomalies.

– GSS

The GSS, known also as the equitable threat score, measures the fraction of observed events that are correctly predicted,
290   adjusted for hits associated with random chance. The GSS does not take in account hits due to chance. It is stricter than the
POD; GSS takes values between $\dfrac{-1}{3}$ and 1. GSS=0 indicates no skill or no correlation while a GSS=1 perfect skill. Given a
contingency table (see [Table2]), the computation of the GSS is done by the following formula:

$$\mathbf{GSS} = \frac{\mathbf{A} - \mathbf{CH}}{\mathbf{A} + \mathbf{B} + \mathbf{C} - \mathbf{H}} \tag{11}$$

With CH given by:

295    $$\mathbf{CH} = \frac{(\mathbf{A} + \mathbf{B})(\mathbf{A} + \mathbf{C})}{\mathbf{A} + \mathbf{B} + \mathbf{C} + \mathbf{D}} \tag{12}$$

3   Results

3.1   Uncertainties in the reanalysis products

The first step of this work consists in assessing the evolution of $T2m$ in the ERA5 and MERRA reanalyses. The climatological
state (annual mean) of $T2m$ in ERA5 and MERRA has been evaluated over the West Africa region from 1 January 1993
300   to 31 December 2020 [Fig3 (a-b)]. Both reanalyses show very similar climatologies of $T2m$: a north-south gradient of the
temperature. The Sahel region appears to be warmer than the Guinean region; this is because of the advection of cold air
coming from the Atlantic ocean to the Guinea coast. This fresh air tends to cool temperatures in this region. The bias between
ERA5 and MERRA is computed using ERA5 as reference [Fig3 c)]. MERRA shows a cold bias with respect to ERA5 over the
Sahel region and Guinean zone except in some countries (e.g., Guinea Bissau, Sierra Leone, Liberia) where we observe a hot
305   bias. Biased values between ERA5 and MERRA are around +/-2°C. The bias highlighted between ERA5 and MERRA is very
significant for heat wave detection. Thereafter, we evaluate the temporal coherence between the two reanalyses by computing
the ACC for $T2m, AT$ and Tw (see [Fig3 (d-i)). We observed a weak correlation over the south of Sahel and Guinean region
around 0.5 (0.7) for max (min) values of $T2m$ and AT (see [Fig3 (d-e) and (g-h)]). This could be explained by the presence
of a strong diurnal cycle in the region associated with high variability during the day and less variability during the night. This
310   will lead to a high variability in the daily max values compared to the daily min values. Tw shows a uniform repartition of
correlation between ERA5 and MERRA around 0.85 except in the Guinean region with max values. Good agreement between
the 2 products is found with Tw. We can infer from this result that Tw has a more stable signal than $T2m$ and AT. Knowing
that heat waves are defined as extreme events, it is important to evaluate the coherence of the reanalysis products on the
representation of extreme values. The hits rate and GSS have been computed in terms of hot days using $T2m$, and we noticed
315   very weak values between the two reanalysis products over the southern Sahel and Guinean region around 0.25 (see [FigS4]
in the supplemental material). Similar results have been found with Tw (not shown). The lack of coherence between ERA5
and MERRA on the representation of hot days would result in discrepancies on the number of heat wave events derived from

the two products. The analysis of heat waves occurrence in the two products using $T2m$ and AT shows big differences over the coastal region (see [FigS5] in the supplemental material). This is very coherent with the results of the ACC correlation shown previously. These discrepancies in the reanalyses ERA5 and MERRA in West Africa have also been highlighted by Engdaw et al. (2022). The potential origins of these differences are explored in the discussion section. The spatial variability of heat waves occurrence in ERA5, using $T2m$ and AT as indicators, is very similar whatever the methods applied for heat waves detection. This strong correlation between T2m and AT is also observed when using MERRA reanalysis (see [FigS6]). Even though the reanalyses present discrepancies over the south of Sahel and coastal region regarding the key variables, the correlation between the variables is preserved.

3.2 Sensitivity of heat wave detection on the threshold values

As we have seen previously in the section "heat wave detection", the threshold value used for heat waves monitoring has a significant impact on the characteristics of the heat waves. The threshold value is generally tailored to the application one wants to achieve. In this part of the work, we investigate the sensitivity of heat waves occurrence on different thresholds. To achieve this goal, we define 4 relative threshold values computed over the entire period: the $75^{th}, 80^{th}, 85^{th}$ and 90th daily percentiles. The choice of these thresholds to evaluate the changes on heat wave detection is based on previous work. Many studies are using the 90th percentile to define a heat wave (e.g., Fischer and Schär, 2010; Perkins et al., 2012a, b; Déqué et al., 2017; Lavaysse et al., 2018; Barbier et al., 2018); other studies are using the 75th percentile (Guigma et al., 2020). Based on these studies, we decided to test the sensitivity of threshold values from the third quartile (75th) to 90th percentile by steps of 5% to quantify significant changes in the frequency of heat wave events. As we are studying extreme events, it is not relevant to go below the third quartile; As we are studying extreme events, it is not relevant to go below the third quartile; knowing also that this study focuses on human impacts of heat waves, the 90th percentile is enough as a maximum threshold. The heat wave detection is processed separately for these 4 thresholds (see [FigS7] in the supplemental material).

The sensitivity on heat waves frequency or duration with respect to the thresholds ($75^{th}, 80^{th}, 85^{th}, 90^{th}$ percentiles) is processed independently for the 4 thresholds; this is done by the computation of the linear evolution coefficient over each grid point. The linear evolution coefficient is defined as the slope of the linear regression line fitted between the threshold values ($Q_{75}, Q_{80}, Q_{85}, Q_{90}$) and the number of events associated to each threshold ($NQ_{75}, NQ_{80}, NQ_{85}, NQ_{90}$) or their corresponding duration ($DQ_{75}, DQ_{80}, DQ_{85}, DQ_{90}$). The computation of the linear evolution coefficient is done by the following steps:

- After processing to heat waves detection at each grid point for the 4 thresholds separately, we compute for each of them the heat waves frequency and duration;

- then fitted a regression line between the threshold values ($Q_{75}, Q_{80}, Q_{85}, Q_{90}$) and their corresponding occurrence or duration. This is done for each grid point;

- Finally, the changes in heat waves occurrence/duration from the 75th to 90th percentiles at each grid point, is given by the computation of the slope of the regression line fitted at step 2 between the threshold values and their corresponding heat waves occurrence/duration.

12

We are aware that this regression based on 4 points is not very robust, nevertheless it makes it possible to obtain information on the evolution of the heat wave characteristics with respect to the thresholds. Therefore, we evaluated the significance of the slope values according to the thresholds using a confidence level of 95%. The significance of the slope has been evaluated using a two sided Chi-square statistics test (Pandis, 2016).

The linear evolution is given by the following equations:

$$\mathbf{N} = \mathbf{a_w} * \mathbf{threshold} + \mathbf{b_w} \tag{13}$$

$$\mathbf{D} = \mathbf{a_w^{'}} * \mathbf{threshold} + \mathbf{b_w^{'}} \tag{14}$$

where $a_w, a_w^{'}$ and $b_w, b_w^{'}$ are respectively the slopes and intercepts of the regressions at the grid point w for heat waves occurrence and duration.

This analysis is conducted with $T2m$ and Tw extracted from MERRA and ERA5 reanalyses. We notice a high spatial variability of the sensitivity of heat waves occurrence to the threshold values over West African regions ([FigS8] and [FigS9] in the supplemental material). Some regions are more sensitive than the others; this can be explained by a strong seasonal cycle of the $T2m$ and Tw signals in those regions. We observe low changes in the heat wave occurrence and duration with respect to the thresholds when using both min and max values of $T2m$ or Tw ([FigS8 (c,f)], [Fig4 (c,f)] and [FigS9 (c,f)] in supplement material); this is related to the small size of the sample of events detected with method 3 (see section heat wave detection for more details). As observed in the results, we can expect the frequency of heat waves to increase when diminishing the values of the threshold (see [FigS8] and [FigS7] in the supplemental material). Heat waves detected using low threshold values are very persistent and last for several days ([Fig4] shows an illustration with $T2m$ used as indicator). This can be explained by the fact that when using a low threshold value, one may expect to have many days with temperature values above the daily threshold. Conversely, for heat waves related to high threshold values, the duration of the events is considerably reduced. This is statistically coherent because the number of consecutive days with temperature above the threshold will decrease as the threshold increases. In general, we find that the duration of heat waves is more sensitive to the threshold values than their frequency of occurrence. This is very coherent because the persistence of a heat wave will be mostly affected by the threshold values used for the detection.

3.3 Sensitivity of heat wave detection to the choice of indicators and methods applied

We have shown that the heat waves detection is very sensitive to threshold values. Based on the literature review and the application of this work, for the rest of the study, we use the 90th percentile for heat wave analyses (e.g., Fischer and Schär, 2010; Perkins et al., 2012a; Perkins and Alexander, 2013; Fontaine et al., 2013; McGregor et al., 2015; Russo et al., 2016; Mutiibwa et al., 2015; Oueslati et al., 2017; Déqué et al., 2017; Batté et al., 2018; Barbier et al., 2018; Lavaysse et al., 2018; Yu et al., 2021; Engdaw et al., 2022) using ERA5 reanalysis [Fig5]. We identified four indicators: $T2m, Tw, AT$ and $UTCI$ from

which heat waves detection has been processed using three different methods (see section methods for more details). We notice that daytime and nighttime heat wave occurrences [Fig5 (a-d);(e-h)] are in the same range of values, while for concomitant events [Fig5 (i-l)], the occurrence of heat waves is drastically reduced by $\frac{1}{4}$. This could be explained by the fact that nighttime and daytime heat waves are not necessarily occuring at the same time and their origins are totally different. Daytime heat waves will be mainly influenced by incoming solar radiation, while nighttime heat waves by the water vapor content in the air mass (Barbier et al., 2018; Largeron et al., 2020). We observe a high occurrence of nighttime heat waves over the coastal region from Guinea to Cameroon [Fig5 (a-d)] linked to moist air coming from the Atlantic ocean in the region during the night; daytime heat waves are more frequent on the Sahel and north-east of Sahara [Fig5 (e-h)] due to hot temperatures over the continental regions. When analysing nighttime heat wave events from each indicator [Fig5 (a-d)], it appears that Tw heat wave events are more frequent than $T2m/AT/UTCI$ events. It appears that Tw is more sensitive to humidity than the other indicators (see formula of Tw); it could explain the high frequency of events observed during the night in the coastal region. Regarding daytime heat waves [Fig5 (e-h)], the spatial variability of events is more consistent for all the indicators in the Sahelian zone. However, some differences are observed: an increase of heat waves occurrence over the coastal region with Tw is noticed in comparison with $T2m, AT$ and $UTCI$. The detection of heat wave events with method 3, show that Tw events are more frequent than $T2m/AT/UTCI$ events with a maximum of occurrence located over the northern Sahel. This means that daytime and nighttime heat waves occur frequently simultaneaously in the Sahel with Tw. We can infer from this result that humidity plays a preponderant role in the occurrence of concomitant heat waves which are very dangerous for human health. In this section, we show the high sensitivity of heat waves detection on the methodology applied and the variables used as indicators. The role of humidity on heat waves occurrence in the coastal region has also been highlighted. Similar results are found with MERRA reanalysis (not shown).

In summary, the heat wave detection is influenced by many parameters: the dataset, threshold values, indicators and methodology used to define such an event. There is a high dependency between these parameters and the climatic region investigated. We show an illustration of the sensitivity of heat wave characteristics to the previous parameters in the CONT region [Fig6], as well as the ATL and GU regions (see [FigS10] and [FigS11] in the supplemental material) using ERA5 and MERRA reanalyses.

3.4 Monitoring of heat waves over West Africa regions

In this section, we analyse the spatial variability of heat wave events in three climate regions (CONT, ATL and GU see section "region of interest" for more details) using $T2m$, AT, Tw as indicators and reanalysis data. Besides ERA5 is slightly better than MERRA when comparing to the stations data [FigS3b], we evaluated the recent evolution of heat waves in the two reanalyses. For this purpose, we evaluate firstly the interannual variability of heat waves and their characteristics from 1993 to 2020. For each region, the characteristics of heat waves have been computed as the ratio of the sum of the characteristics of all the cities belonging to a region divided by the number of cities. We identified some particular hot years with a high frequency of nighttime, daytime and concomitant heat waves: 1998, 2005, 2010, 2016 2019 and 2020 in the 3 regions for all the indicators (see [Fig7], [FigS12 and FigS13] in the supplemental material). These years with peaks of heat waves are

addressed in the discussion section. It appears that the GU region experiences more heat waves during the last decade compared to the CONT and ATL regions (see [FigS12] for daytime events and [FigS13] for nighttime in the supplemental material). The mean duration of heat waves detected in the three regions are in the same range of values with some specific persistent events at the end of the period in the ATL and GU regions (not shown). Strong and more persistent heat wave events are found in the CONT region. From a statistical point of view, this is due to less variability in the signal of indicators in the region which favor the detection of consecutive days with values of indicators above the threshold. Highest occurences of heat waves in the three regions are associated to Tw for daytime and nighttime events (see [FigS12] and [FigS13] respectively). Conversely, heat waves events with high intensity are found with AT (not shown) in the three regions. We can infer from this result that AT presents a more stable signal in the regions than $T2m$ and Tw. Strong intensity concomitant events are found in the CONT and ATL regions (see [FigS15] in the supplemental material).

We also investigate the seasonal distribution of heat waves occurrence in the 3 regions. We notice an increase of the frequency of daytime and nighttime heat waves events at the beginning of the season and during the retreat period of the West Africa monsoon (starting in September, see [FigS14 (a-c)] in supplement material). A decrease in heat wave frequency is observed during the monsoon activity phase in the 3 regions; this is coherent because the monsoon flux brings rainfall in the region leading to a cooling effect. Concomitant heat waves show a seasonal cycle with strong fluctuations [FigS16]. This is explained by the fact that concomitant events are conditioned by daytime and nighttime heat waves which are two distinct processes.

The seasonal cycle of the duration and intensity of heat waves follows the same distribution as the heat wave occurrence (see [Fig8 (a-c)] and [Fig8 (d-f)] respectively). Persistent and strong intensity heat waves (nighttime, daytime) are taking place at the beginning and the end of the season, while short term and weak intensity events are occurring during the monsoon phase ([Fig8 (a-c)], [Fig8 (d-f)]). This is verified for all the 3 indicators in spite of some discrepancies. The period 1993-2020 is then divided into 3 three decades : [1993-2001], [2002-2011] and [2012-2020]; and we evaluate the contribution of each decade on the heat wave characteristics over the whole period (see [Fig9 (a,b,c) - (g,h,i)] for heat waves duration). Results are similar when analyzing the intensity of heat waves (not shown). The percentiles used for the detection of heat waves in each decade are computed over the whole period 1993-2020. It is clearly shown with ERA5 that the major contribution on heat wave characteristics over the period is coming from the last decade [Fig9 (g,h,i)]. We notice a progressive increase in frequency, duration and intensity of all the heat waves (daytime, nighttime and concomitant) from the first to the last decade in the 3 regions (see [FigS14(j-l)] and [FigS16 (j-l)] in the supplemental material); this is true for all the indicators. When using ERA5 reanalysis, we found the last decade [2012-2020] shows a major contribution around 50% of heat wave characteristics over the period 1993-2010, while the first and second decades contribute up to 22.4% and 27.6% respectively. This contribution of the last decade over the total period is not effective in MERRA reanalysis for which all the three decades seem to have similar contribution. This is a result of the uncertainties highlighted previously in the two reanalyses. The reinforcement of extreme events such as heat waves during the last decade in ERA5 is possibly being linked to global warming. This result is in agreement with other studies which show an increase of heat waves frequency and property under climate change (e.g., Dosio, 2017; Dosio et al., 2018; Murari and Ghosh, 2019; Lorenzo et al., 2021; Engdaw et al., 2022). When analysing the severity

of heat waves over the previous decades using the mean duration and intensity (see [FigS17] and [FigS18]), we do not find a significant increase of heat wave characteristics over the 3 decades.

450   After assessing the temporal evolution of heat waves over the 3 regions, we analyse their persistence based on their duration using ERA5 and MERRA reanalyses and maximum values of the indicators (see [Fig10] and [FigS19] respectively). We defined 5 types of events as described in [Table3]). We observed that approximately 75% of daytime heat waves have a duration of 3-6 days with at least 40% of events belonging to C1 [Fig10]. Very persistent daytime heat waves contribute to at least 9-13% of the events registered. Severe and very severe daytime events are extremely rare in the region; and they contribute up to 12% of
455   the total number of heat waves. The classification is not too sensitive to the indicators and the regions. We obtained a similar classification with nighttime heat waves (not shown).

4   Discussion on the uncertainties found in reanalyses and the impact of the SST in the Atlantic

We analyse the evolution of heat waves occurrence and characteristics over a variety of climatic regions in West Africa. The spatial variability of heat wave indicators ($T2m$ and Tw) over West Africa during the seasons (winter, spring, summer and
460   autumn) has been investigated. This is done through the computation of the interannual daily standard deviation over the period 1993-2020. We find lowest values of standard deviation over the 3 regions of interest (CONT, ATL and GU) during the summer and autumn when using min values of $T2m(T2m_{min})$ (see [FigS20] in the supplement material). This shows a weak variability in the signal of $T2m_{min}$ which indicate favorable conditions for the occurrence of persistent heat waves in these regions during this period. With Tw, there is a weak variability of the signal during the summer for both min and max values indicative of
465   persistent events. We find some discrepancies in the reanalysis products ERA5 and MERRA. The results show that ERA5 appears to be hotter than MERRA over the Sahel region. The source of these discrepancies in the reanalyses is very complex and can result from various factors such as the data assimilation techniques ($4D - Var$ (Bonavita et al., 2016) for ERA5 and $3D - Var$ (Courtier et al., 1998) for MERRA), atmospheric models, convective schemes, bias correction methods, spatial resolution and model parameterisation. Another big difference between ERA5 and MERRA is found in the vertical resolution
470   of the profiles of the atmospheric variables between 0-2 km; ERA5 has more atmospheric vertical levels than MERRA below 2 km which leads to more accurate representation of processes in the boundary layer (Taszarek et al., 2021). Many studies highlighted these differences in the 2 reanalysis products (e.g., Olauson, 2018; Graham et al., 2019; Taszarek et al., 2021); some authors (e.g., Gensini et al., 2014; Tippett et al., 2014; Allen et al., 2015; Taszarek et al., 2018; King and Kennedy, 2019) identified the model parameterisation and data assimilation technique as possible causes of biases in reanalyses for low level
475   thermodynamic fields. The investigation in more detail of the source of these uncertainties is out of the scope of this paper.

An assessment of the origins of heat waves in the West African coastal regions is discussed. One driver of heat waves over the globe highlighted by many studies, is the "blocking high" (e.g., Charney and DeVore, 1979; Coughlan, 1983; Perkins, 2015). This situation happens when a high pressure system remains in the same region for a longer period than what is

usually expected. The consequence of this phenomenon is the compression of the air mass at the surface leading to an increase
of temperatures in the region. Perkins (2015) also identified soil moisture-atmosphere interactions and large-scale climate
dynamics as other drivers of heat waves.

To address the origin of heat waves in the coastal region, we firstly analysed the interannual variability of the Sea Surface
Temperature (SST) over the period 1993-2020 using ERA5 reanalysis. We computed the mean anomalies of SST with respect
to the climatology [FigS21]. A warming over the north-eastern and south-eastern tropical Atlantic ocean is observed during
specific years: 1998, 2005, 2008, 2010, 2016, 2019 and 2020. This warming over the tropical Atlantic ocean is affecting all
the western Africa coastal region. In comparison with the interannual variability of heat waves occurrence in the coastal region
(see [FigS12] in the supplemental material), we noticed that the years of high frequency of heat waves correspond to the years
during which a warming of the ocean was observed : 1998, 2005, 2010, 2016 , 2019 and 2020 for instance. These years also
correspond to the occurrence of El nino events. The link between the SST and heat waves has been investigated in more detail
in the following. We computed the yearly mean SST anomalies with respect to heat waves days using the formula below :

$$\mathbf{Ano\_SST\_year} = \sum_{i=1}^{12} \alpha_i * \mathbf{Ano_i} = \alpha_1 * \mathbf{Ano_1} + \alpha_2 * \mathbf{Ano_2} + \alpha_3 * \mathbf{Ano_3} + ... + \alpha_{12} * \mathbf{Ano_{12}} \tag{15}$$

Where α_i represents the total number of days in heat waves per month for each year, if there is no event detected then $\alpha_i = 0$.

For this analysis, we focused on the years with high peaks of heat waves identified previously (1998, 2005, 2008, 2010,
2016, 2019 and 2020) using $T2m$ as indicator for heat waves detection. We noticed that most of the heat waves are associated
with a warming of the tropical Atlantic ocean except for some specific years such as 2016 and 2019 in the GU and ATL regions
respectively [Figure11 (a,b)]. In the CONT region, heat waves are influenced by both the west-east air flow coming from the
tropical north Atlantic ocean and the south-north air flow coming from the tropical south Atlantic ocean [Figure11 (c,d)]. Some
years with a considerable number of heat waves detected are not associated to positive anomalies of SST. These heat waves are
occurring during a cold phase of the tropical Atlantic ocean. There is no major changes observed in the analysis when using
AT and Tw as indicators for heat waves detection (not shown). We can suggest from this result that heat waves in the coastal
region have many drivers, and one of them at local scale could be the oceanic forcings through the SST. Large scale (El nino,
atmospheric circulation) and local scale (soil-moisture interactions) processes may also contribute to the occurrence of heat
waves in the region. This result is in agreement with Russo et al. (2016) and Moron et al. (2016) who identified links between
heat waves and El niño events. The investigation of the physical processes driving heat waves in the coastal region required
more in-depth knowledge of local and large-scale forcings, which is beyond the scope of this paper.

5 Conclusions

The present work assesses the potential uncertainties associated with heat waves detection using reanalysis data (ERA5,
MERRA). It also looks into the recent evolution of heat waves in different parts of the West Africa region.

The first uncertainty highlighted in this study is coming from the reanalyses ERA5 and MERRA. We found biases in the reanalysis products; MERRA shows a cold bias with respect to ERA5 over the Sahel region and the Guinean region except over some countries (Guinea Bissau, Sierra Leone, Liberia). Weak correlations between ERA5 and MERRA have been found over the Guinea coast using min/max values of $T2m$ and AT indicators. The representation of extreme values in the reanalyses has been analyzed, evidencing that the coherence between the 2 products is very low, around 0.25, in the southern Sahel and the Guinean region. This low agreement between the 2 reanalyses results in discrepancies on the frequency of heat waves associated with each product. Even though the reanalyses present large discrepancies over the South Sahel and Guinea coast, they are able to preserve the relationship between the variables used to detect heat waves (AT, $T2m$). The interpolated temperatures from local station in Dakar and Abidjan, show slightly better correlation with ERA5 than MERRA. The second uncertainty found here, is the sensitivity of the spatial variability of heat waves to the threshold values used to process the monitoring of events. Heat waves detected using low threshold values of the indicators $T2m$ and Tw are very persistent and last for several days, while the duration of heat waves related to the high threshold values is considerably reduced. We notice some discrepancies in the sensitivity to the threshold values of heat waves detected with Tw and $T2m$. Nighttime and daytime heat waves are in the same range of occurrence while concomitant events are extremely rare because they are more restrictive. This shows daytime and nighttime heat waves are distinct phenomena. The climatological state of heat wave occurrence shows large differences between the indicators. Nighttime heat waves associated to Tw are more frequent than the ones detected with AT, $T2m$, $UTCI$. Humidity plays an important role in nighttime events and tends to reinforce concomitant events over the north Sahel. The spatial variability of daytime heat waves is more consistent for all the indicators over the Sahelian zone. The interannual variability of heat waves in the west Africa coastal region shows for the 3 indicators (AT, $T2m$, Tw) some particularly hotter years with high frequency of events : $1998, 2005, 2010, 2016, 2019$ and 2020 linked to El Niño events. The GU region is more affected by heat waves during the last decade (2012-2020) than the CONT and ATL regions. The CONT region experienced more persistent and stronger intensity heat waves than the GU region. The seasonal cycle of heat waves shows an increase of the frequency of the events at the beginning of the season and during the retreat phase of the west African monsoon. Conversely, a decrease of heat waves occurrence is observed during the monsoon activity period in the 3 regions. We observed a reinforcement in the frequency, duration and intensity of heat waves during the last decade (2012-2020). This is a consequence of global warming acting on extreme events. No significant changes on the severity of heat waves have been found in the regions during the 3 decades. Most of the events detected in the regions (75%) have a duration around 3-6 days. The most dangerous events with a duration of at least 10 days contributed up to 12% of the total number of events. We noticed strong links between SST and heat waves during some specific years of peaks of events but this is not the case for 2016 and 2019 in the GU and ATL regions respectively. We can infer from this result that there is a contribution of oceanic forcings in the reinforcement of heat waves in the coastal region among many other drivers. In a future work, we will investigate in more detail the influence of large-scale forcings on heat waves occurrence in this region. In the present study, we detected different types of heat waves based on the methodology and indicator used, it will be very important to investigate their potential impacts on human health and their activities.

545 References

Alduchov, O. A. and Eskridge, R. E.: Improved Magnus form approximation of saturation vapor pressure, Journal of Applied Meteorology and Climatology, 35, 601–609, 1996.

Allen, J. T., Tippett, M. K., and Sobel, A. H.: An empirical model relating US monthly hail occurrence to large-scale meteorological environment, Journal of Advances in Modeling Earth Systems, 7, 226–243, 2015.

550 Anderson, B. G. and Bell, M. L.: Weather-Related Mortality, 20, 205–213, https://doi.org/10.1097/EDE.0b013e318190ee08, 2009.

August, E. F.: Ueber die Berechnung der Expansivkraft des Wasserdunstes, 89, 122–137, https://doi.org/10.1002/andp.18280890511, _eprint: https://onlinelibrary.wiley.com/doi/pdf/10.1002/andp.18280890511, 1828.

Barbier, J., Guichard, F., Bouniol, D., Couvreux, F., and Roehrig, R.: Detection of Intraseasonal Large-Scale Heat Waves: Characteristics and Historical Trends during the Sahelian Spring, 31, 61–80, https://doi.org/10.1175/JCLI-D-17-0244.1, publisher: American Meteorological 555 Society Section: Journal of Climate, 2018.

Batté, L., Ardilouze, C., and Déqué, M.: Forecasting West African Heat Waves at Subseasonal and Seasonal Time Scales, 146, 889–907, https://doi.org/10.1175/MWR-D-17-0211.1, publisher: American Meteorological Society Section: Monthly Weather Review, 2018.

Beniston, M., Stoffel, M., and Guillet, S.: Comparing observed and hypothetical climates as a means of communicating to the public and policymakers: The case of European heatwaves, 67, 27–34, https://doi.org/10.1016/j.envsci.2016.11.008, 2017.

560 Bonavita, M., Hólm, E., Isaksen, L., and Fisher, M.: The evolution of the ECMWF hybrid data assimilation system, 142, 287–303, https://doi.org/10.1002/qj.2652, _eprint: https://onlinelibrary.wiley.com/doi/pdf/10.1002/qj.2652, 2016.

Braga, A. L. F., Zanobetti, A., and Schwartz, J.: The effect of weather on respiratory and cardiovascular deaths in 12 U.S. cities., 110, 859–863, https://doi.org/10.1289/ehp.02110859, publisher: Environmental Health Perspectives, 2002.

Buck, A. L.: New equations for computing vapor pressure and enhancement factor, Journal of Applied Meteorology and Climatology, 20, 565 1527–1532, 1981.

Ceccherini, G., Russo, S., Ameztoy, I., Marchese, A. F., and Carmona-Moreno, C.: Heat waves in Africa 1981–2015, observations and reanalysis, 17, 115–125, https://doi.org/10.5194/nhess-17-115-2017, 2017.

Charney, J. G. and DeVore, J. G.: Multiple flow equilibria in the atmosphere and blocking, Journal of Atmospheric Sciences, 36, 1205–1216, 1979.

570 Coughlan, M.: A comparative climatology of blocking action in the two hemispheres, Australian meteorological magazine Melbourne, 31, 3–13, 1983.

Courtier, P., Andersson, E., Heckley, W., Vasiljevic, D., Hamrud, M., Hollingsworth, A., Rabier, F., Fisher, M., and Pailleux, J.: The ECMWF implementation of three-dimensional variational assimilation (3D-Var). I: Formulation, 124, 1783–1807, https://doi.org/10.1002/qj.49712455002, _eprint: https://onlinelibrary.wiley.com/doi/pdf/10.1002/qj.49712455002, 1998.

575 Déqué, M., Calmanti, S., Christensen, O. B., Aquila, A. D., Maule, C. F., Haensler, A., Nikulin, G., and Teichmann, C.: A multi-model climate response over tropical Africa at+ 2° C, Climate Services, 7, 87–95, 2017.

Di Napoli, C., Barnard, C., Prudhomme, C., Cloke, H. L., and Pappenberger, F.: ERA5-HEAT: A global gridded historical dataset of human thermal comfort indices from climate reanalysis, 8, 2–10, https://doi.org/10.1002/gdj3.102, _eprint: https://onlinelibrary.wiley.com/doi/pdf/10.1002/gdj3.102, 2021.

580 Dosio, A.: Projection of temperature and heat waves for Africa with an ensemble of CORDEX Regional Climate Models, 49, 493–519, https://doi.org/10.1007/s00382-016-3355-5, 2017.

Dosio, A., Mentaschi, L., Fischer, E. M., and Wyser, K.: Extreme heat waves under 1.5\hspace0.167em°C and 2\hspace0.167em°C global warming, 13, 054 006, https://doi.org/10.1088/1748-9326/aab827, publisher: IOP Publishing, 2018.

Engdaw, M. M., Ballinger, A. P., Hegerl, G. C., and Steiner, A. K.: Changes in temperature and heat waves over Africa using observational and reanalysis data sets, International Journal of Climatology, 42, 1165–1180, 2022.

Fischer, E. M. and Schär, C.: Consistent geographical patterns of changes in high-impact European heatwaves, Nature geoscience, 3, 398–403, 2010.

Fontaine, B., Janicot, S., and Monerie, P.-A.: Recent changes in air temperature, heat waves occurrences, and atmospheric circulation in Northern Africa, 118, 8536–8552, https://doi.org/10.1002/jgrd.50667, _eprint: https://onlinelibrary.wiley.com/doi/pdf/10.1002/jgrd.50667, 2013.

Fouillet, A., Rey, G., Laurent, F., Pavillon, G., Bellec, S., Guihenneuc-Jouyaux, C., Clavel, J., Jougla, E., and Hémon, D.: Excess mortality related to the August 2003 heat wave in France, 80, 16–24, https://doi.org/10.1007/s00420-006-0089-4, 2006.

Gasparrini, A. and Armstrong, B.: The impact of heat waves on mortality, 22, 68–73, https://doi.org/10.1097/EDE.0b013e3181fdcd99, 2011.

Gelaro, R., McCarty, W., Suárez, M. J., Todling, R., Molod, A., Takacs, L., Randles, C. A., Darmenov, A., Bosilovich, M. G., Reichle, R., Wargan, K., Coy, L., Cullather, R., Draper, C., Akella, S., Buchard, V., Conaty, A., Silva, A. M. d., Gu, W., Kim, G.-K., Koster, R., Lucchesi, R., Merkova, D., Nielsen, J. E., Partyka, G., Pawson, S., Putman, W., Rienecker, M., Schubert, S. D., Sienkiewicz, M., and Zhao, B.: The Modern-Era Retrospective Analysis for Research and Applications, Version 2 (MERRA-2), 30, 5419–5454, https://doi.org/10.1175/JCLI-D-16-0758.1, publisher: American Meteorological Society Section: Journal of Climate, 2017.

Gensini, V. A., Mote, T. L., and Brooks, H. E.: Severe-thunderstorm reanalysis environments and collocated radiosonde observations, Journal of Applied Meteorology and Climatology, 53, 742–751, 2014.

Gleixner, S., Demissie, T., and Diro, G. T.: Did ERA5 improve temperature and precipitation reanalysis over East Africa?, Atmosphere, 11, 996, 2020.

Graham, R. M., Hudson, S. R., and Maturilli, M.: Improved performance of ERA5 in Arctic gateway relative to four global atmospheric reanalyses, Geophysical Research Letters, 46, 6138–6147, 2019.

Guigma, K. H., Todd, M., and Wang, Y.: Characteristics and thermodynamics of Sahelian heatwaves analysed using various thermal indices, 55, 3151–3175, https://doi.org/10.1007/s00382-020-05438-5, 2020.

Hajat, S., Kovats, R. S., and Lachowycz, K.: Heat-related and cold-related deaths in England and Wales: who is at risk?, 64, 93–100, https://doi.org/10.1136/oem.2006.029017, publisher: BMJ Publishing Group Ltd Section: Original article, 2007.

Hartmann, D. L., Tank, A. M. K., Rusticucci, M., Alexander, L. V., Brönnimann, S., Charabi, Y. A. R., Dentener, F. J., Dlugokencky, E. J., Easterling, D. R., Kaplan, A., et al.: Observations: atmosphere and surface, in: Climate change 2013 the physical science basis: Working group I contribution to the fifth assessment report of the intergovernmental panel on climate change, pp. 159–254, Cambridge University Press, 2013.

Hersbach, H., Bell, B., Berrisford, P., Hirahara, S., Horányi, A., Muñoz-Sabater, J., Nicolas, J., Peubey, C., Radu, R., Schepers, D., Simmons, A., Soci, C., Abdalla, S., Abellan, X., Balsamo, G., Bechtold, P., Biavati, G., Bidlot, J., Bonavita, M., De Chiara, G., Dahlgren, P., Dee, D., Diamantakis, M., Dragani, R., Flemming, J., Forbes, R., Fuentes, M., Geer, A., Haimberger, L., Healy, S., Hogan, R. J., Hólm, E., Janisková, M., Keeley, S., Laloyaux, P., Lopez, P., Lupu, C., Radnoti, G., de Rosnay, P., Rozum, I., Vamborg, F., Villaume, S., and Thépaut, J.-N.: The ERA5 global reanalysis, 146, 1999–2049, https://doi.org/10.1002/qj.3803, _eprint: https://onlinelibrary.wiley.com/doi/pdf/10.1002/qj.3803, 2020.

Huynen, M. M., Martens, P., Schram, D., Weijenberg, M. P., and Kunst, A. E.: The impact of heat waves and cold spells on mortality rates in the Dutch population., 109, 463–470, https://doi.org/10.1289/ehp.01109463, publisher: Environmental Health Perspectives, 2001.

King, A. T. and Kennedy, A. D.: North American supercell environments in atmospheric reanalyses and RUC-2, Journal of Applied Meteorology and Climatology, 58, 71–92, 2019.

Kovats, R. S. and Hajat, S.: Heat Stress and Public Health: A Critical Review, 29, 41–55, https://doi.org/10.1146/annurev.publhealth.29.020907.090843, 2008.

Largeron, Y., Guichard, F., Roehrig, R., Couvreux, F., and Barbier, J.: The April 2010 North African heatwave: when the water vapor greenhouse effect drives nighttime temperatures, 54, 3879–3905, https://doi.org/10.1007/s00382-020-05204-7, 2020.

Lavaysse, C., Cammalleri, C., Dosio, A., van der Schrier, G., Toreti, A., and Vogt, J.: Towards a monitoring system of temperature extremes in Europe, 18, 91–104, https://doi.org/10.5194/nhess-18-91-2018, publisher: Copernicus GmbH, 2018.

Lorenzo, N., Díaz-Poso, A., and Royé, D.: Heatwave intensity on the Iberian Peninsula: Future climate projections, 258, 105 655, https://doi.org/10.1016/j.atmosres.2021.105655, 2021.

Loughnan, M.: Heatwaves are silent killers, Geodate, 27, 7–10, 2014.

Magnus, G.: Versuche über die Spannkräfte des Wasserdampfs, 137, 225–247, https://doi.org/10.1002/andp.18441370202, _eprint: https://onlinelibrary.wiley.com/doi/pdf/10.1002/andp.18441370202, 1844.

McGregor, G. R., Bessmoulin, P., Ebi, K., and Menne, B.: Heatwaves and health: guidance on warning-system development., WMOP, 2015.

Moron, V., Oueslati, B., Pohl, B., Rome, S., and Janicot, S.: Trends of mean temperatures and warm extremes in northern tropical Africa (1961–2014) from observed and PPCA-reconstructed time series, Journal of Geophysical Research: Atmospheres, 121, 5298–5319, 2016.

Murari, K. K. and Ghosh, S.: Future Heat Wave Projections and Impacts, in: Climate Change Signals and Response: A Strategic Knowledge Compendium for India, edited by Venkataraman, C., Mishra, T., Ghosh, S., and Karmakar, S., pp. 91–107, Springer, https://doi.org/10.1007/978-981-13-0280-0_6, 2019.

Mutiibwa, D., Vavrus, S. J., McAfee, S. A., and Albright, T. P.: Recent spatiotemporal patterns in temperature extremes across conterminous United States, Journal of Geophysical Research: Atmospheres, 120, 7378–7392, 2015.

Ngoungue Langue, C. G., Lavaysse, C., Vrac, M., Peyrille, P., and Flamant, C.: Seasonal forecasts of the Saharan Heat Low characteristics: A multi-model assessment, Weather and Climate Dynamics, 2, 893–912, 2021.

Olauson, J.: ERA5: The new champion of wind power modelling?, Renewable energy, 126, 322–331, 2018.

Oueslati, B., Pohl, B., Moron, V., Rome, S., and Janicot, S.: Characterization of Heat Waves in the Sahel and Associated Physical Mechanisms, 30, 3095–3115, https://doi.org/10.1175/JCLI-D-16-0432.1, publisher: American Meteorological Society Section: Journal of Climate, 2017.

Pandis, N.: The chi-square test, American journal of orthodontics and dentofacial orthopedics, 150, 898–899, 2016.

Perkins, S. E.: A review on the scientific understanding of heatwaves—Their measurement, driving mechanisms, and changes at the global scale, 164-165, 242–267, https://doi.org/10.1016/j.atmosres.2015.05.014, 2015.

Perkins, S. E. and Alexander, L. V.: On the Measurement of Heat Waves, 26, 4500–4517, https://doi.org/10.1175/JCLI-D-12-00383.1, publisher: American Meteorological Society Section: Journal of Climate, 2013.

Perkins, S. E., Alexander, L. V., and Nairn, J. R.: Increasing frequency, intensity and duration of observed global heatwaves and warm spells, 39, https://doi.org/10.1029/2012GL053361, _eprint: https://onlinelibrary.wiley.com/doi/pdf/10.1029/2012GL053361, 2012a.

Perkins, S. E., Alexander, L. V., and Nairn, J. R.: Increasing frequency, intensity and duration of observed global heatwaves and warm spells, 39, https://doi.org/10.1029/2012GL053361, _eprint: https://onlinelibrary.wiley.com/doi/pdf/10.1029/2012GL053361, 2012b.

Ramon, J., Lledó, L., Torralba, V., Soret, A., and Doblas-Reyes, F. J.: What global reanalysis best represents near-surface winds?, Quarterly Journal of the Royal Meteorological Society, 145, 3236–3251, 2019.

Robinson, P. J.: On the Definition of a Heat Wave, 40, 762–775, https://doi.org/10.1175/1520-0450(2001)040<0762:OTDOAH>2.0.CO;2, publisher: American Meteorological Society Section: Journal of Applied Meteorology and Climatology, 2001.

Rocklöv, J., Forsberg, B., Ebi, K., and Bellander, T.: Susceptibility to mortality related to temperature and heat and cold wave duration in the population of Stockholm County, Sweden, 7, 22 737, https://doi.org/10.3402/gha.v7.22737, publisher: Taylor & Francis _eprint: https://doi.org/10.3402/gha.v7.22737, 2014.

Russo, S., Marchese, A. F., Sillmann, J., and Immé, G.: When will unusual heat waves become normal in a warming Africa?, 11, 054 016, https://doi.org/10.1088/1748-9326/11/5/054016, publisher: IOP Publishing, 2016.

Shafiei Shiva, J., Chandler, D. G., and Kunkel, K. E.: Localized Changes in Heat Wave Properties Across the United States, 7, 300–319, https://doi.org/10.1029/2018EF001085, _eprint: https://onlinelibrary.wiley.com/doi/pdf/10.1029/2018EF001085, 2019.

Shaposhnikov, D., Revich, B., Bellander, T., Bedada, G. B., Bottai, M., Kharkova, T., Kvasha, E., Lezina, E., Lind, T., Semutnikova, E., and Pershagen, G.: Mortality Related to Air Pollution with the Moscow Heat Wave and Wildfire of 2010, 25, 359–364, https://doi.org/10.1097/EDE.0000000000000090, 2014.

Smith, T. T., Zaitchik, B. F., and Gohlke, J. M.: Heat waves in the United States: definitions, patterns and trends, 118, 811–825, https://doi.org/10.1007/s10584-012-0659-2, 2013.

Steadman, R. G.: The Assessment of Sultriness. Part I: A Temperature-Humidity Index Based on Human Physiology and Clothing Science, 18, 861–873, https://doi.org/10.1175/1520-0450(1979)018<0861:TAOSPI>2.0.CO;2, publisher: American Meteorological Society Section: Journal of Applied Meteorology and Climatology, 1979a.

Steadman, R. G.: The Assessment of Sultriness. Part II: Effects of Wind, Extra Radiation and Barometric Pressure on Apparent Temperature, 18, 874–885, https://www.jstor.org/stable/26179217, publisher: American Meteorological Society, 1979b.

Steadman, R. G.: A universal scale of apparent temperature, Journal of Applied Meteorology and Climatology, 23, 1674–1687, 1984.

Stefanon, M., D'Andrea, F., and Drobinski, P.: Heatwave classification over Europe and the Mediterranean region, 7, 014 023, https://doi.org/10.1088/1748-9326/7/1/014023, publisher: IOP Publishing, 2012.

Stull, R.: Wet-Bulb Temperature from Relative Humidity and Air Temperature, 50, 2267–2269, https://doi.org/10.1175/JAMC-D-11-0143.1, publisher: American Meteorological Society Section: Journal of Applied Meteorology and Climatology, 2011.

Tan, J., Zheng, Y., Tang, X., Guo, C., Li, L., Song, G., Zhen, X., Yuan, D., Kalkstein, A. J., Li, F., and Chen, H.: The urban heat island and its impact on heat waves and human health in Shanghai, 54, 75–84, https://doi.org/10.1007/s00484-009-0256-x, 2010.

Taszarek, M., Brooks, H. E., Czernecki, B., Szuster, P., and Fortuniak, K.: Climatological aspects of convective parameters over Europe: A comparison of ERA-Interim and sounding data, Journal of Climate, 31, 4281–4308, 2018.

Taszarek, M., Pilguj, N., Allen, J. T., Gensini, V., Brooks, H. E., and Szuster, P.: Comparison of convective parameters derived from ERA5 and MERRA-2 with rawinsonde data over Europe and North America, Journal of Climate, 34, 3211–3237, 2021.

Tippett, M. K., Sobel, A. H., Camargo, S. J., and Allen, J. T.: An empirical relation between US tornado activity and monthly environmental parameters, Journal of Climate, 27, 2983–2999, 2014.

Wang, P., Tang, J., Sun, X., Liu, J., and Juan, F.: Spatiotemporal characteristics of heat waves over China in regional climate simulations within the CORDEX-EA project, 52, 799–818, https://doi.org/10.1007/s00382-018-4167-6, 2019.

Wehner, M., Castillo, F., and Stone, D.: The impact of moisture and temperature on human health in heat waves, in: Oxford Research Encyclopedia of Natural Hazard Science, 2017.

695   Wu, W.-S., Purser, R. J., and Parrish, D. F.: Three-dimensional variational analysis with spatially inhomogeneous covariances, Monthly Weather Review, 130, 2905–2916, 2002.

Yu, S., Tett, S. F. B., Freychet, N., and Yan, Z.: Changes in regional wet heatwave in Eurasia during summer (1979–2017), 16, 064 094, https://doi.org/10.1088/1748-9326/ac0745, publisher: IOP Publishing, 2021.

Tables

Table 1. Land sea mask (lsm) of west African towns used in this study

Towns	latitude	longitude	lsm
DAKAR	14.75	-17.25	0.6
ABIDJAN	5.25	-3.75	0.5
NOUAKCHOTT	18	-16	continent
CONAKRY	9.5	-13.5	0.5
MONROVIA	6.25	-10.75	0.6
BAMAKO	12.5	-8	continent
YAMOUSSOUKRO	6.75	-5.25	continent
OUAGADOUGOU	12.25	-1.5	continent
ACCRA	5.5	-0.5	0.8
LOMÉ	6	1	0.5
NIAMEY	13.5	2	continent
COTONOU	6.5	2.5	0.7
LAGOS	6.5	3.5	0.5
ABUJA	9	7.5	continent
DOUALA	4	9.75	0.9

Table 2. Contingency table.

2X2 Contingency table		Event Observed	
		YES	N0
Event forecast	YES	A	B
	NO	C	D

Table 3. Classification of heat waves based on the duration.

Classes	Duration (days)	Degree of persistence
C1	3	normal
C2	4-6	persistent
C3	7-9	very persistent
C4	10-12	severe
C5	+13	very severe
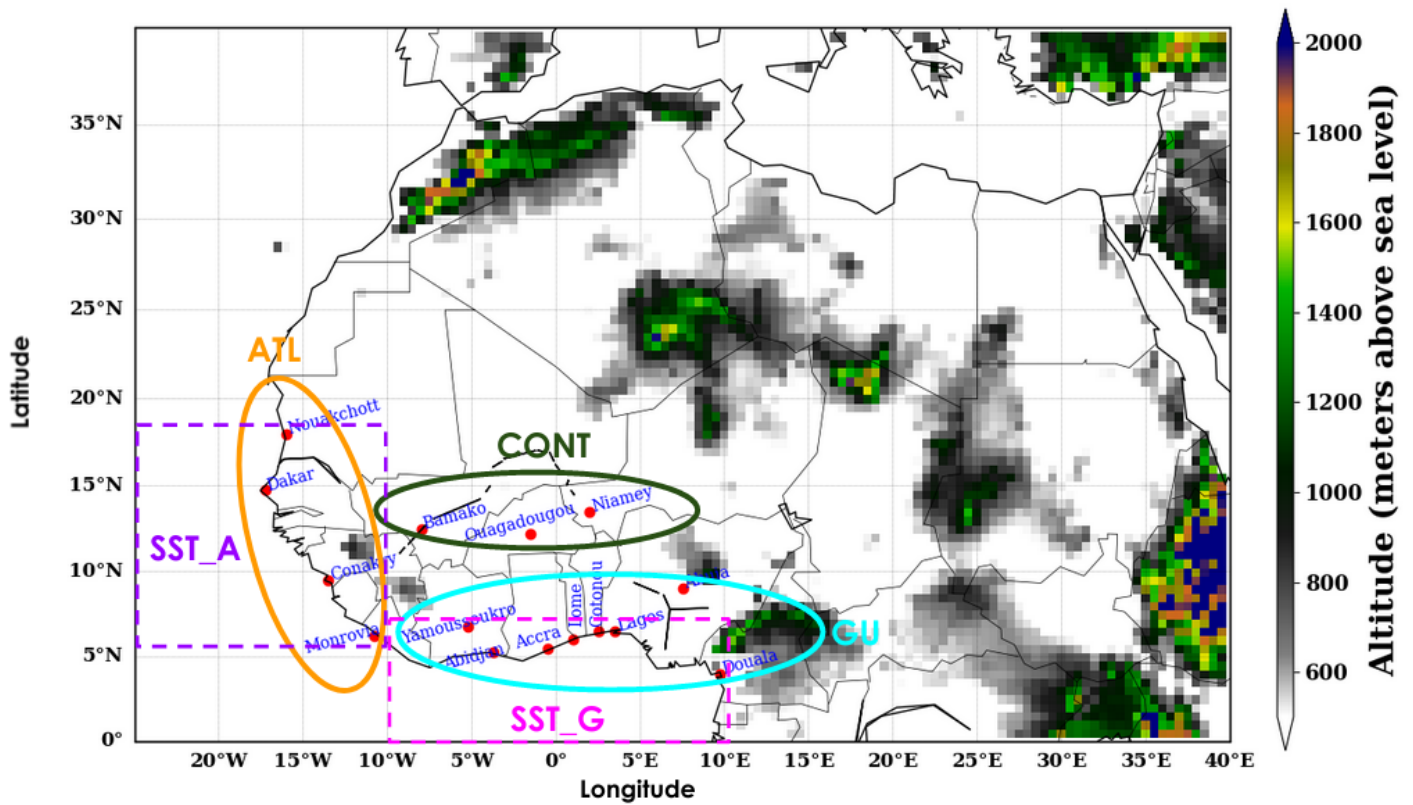
Figure 1. *Topographic map of West Africa using ERA5 elevation data. The circles on the map represent the different climatic zones:* ***ATL*** *(Coastal atlantic zone),* ***CONT*** *(Continental zone) and* ***GU*** *(Coastal Guinean zone). The two boxes namely* ***SST_A*** *and* ***SST_G*** *represent the boxes used to analyze the links between Sea Surface Temperature (SST) and heat waves for the ATL and GU regions respectively. The Y- and X- axis represent the latitude and longitude respectively. The color bar shows the elevation in meters over the region.*
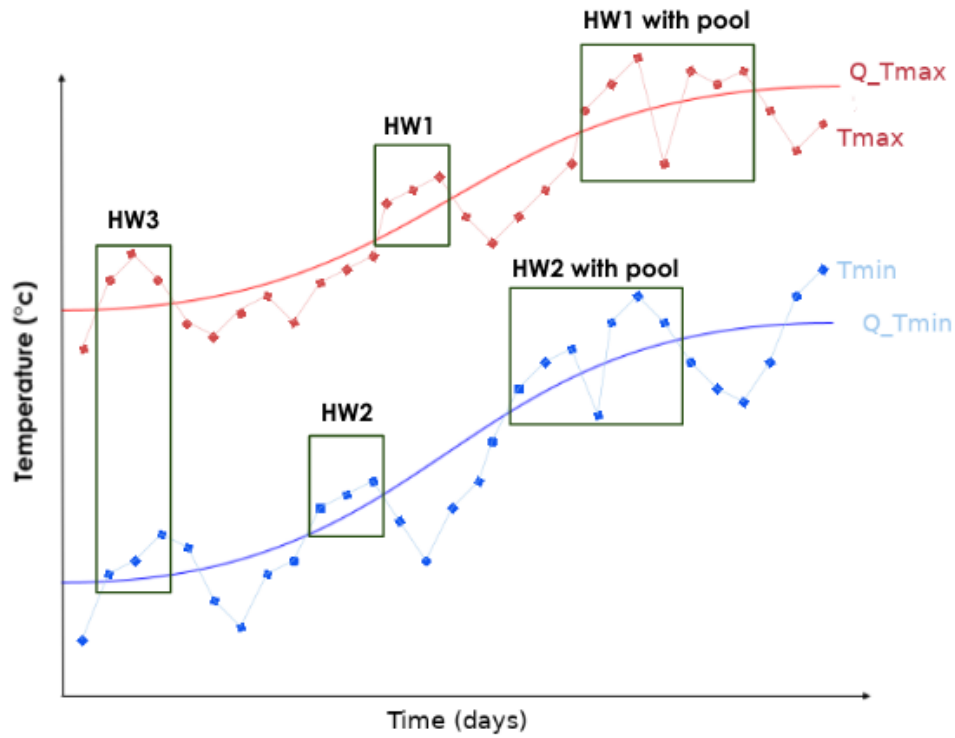
Figure 2. *Detection process of heat wave:* **HW1/HW2** *represent events associated respectively to maxima/minima temperature,* **HW3** *are events detected at the same time in maxima and minima temperatures. The red/blue lines with circles are max/min daily temperatures. Red/blue solid lines are max/min thresholds respectively. X- and Y- axis represent the time in days and the temperature in degrees Celsius respectively. 'With pool' refers to the pooling of two (or more) events separated by a day characterized by the value of a given indicator below the daily XXth percentile. This figure is a 'schematic' illustration of the different types of heat waves investigated in this work.*
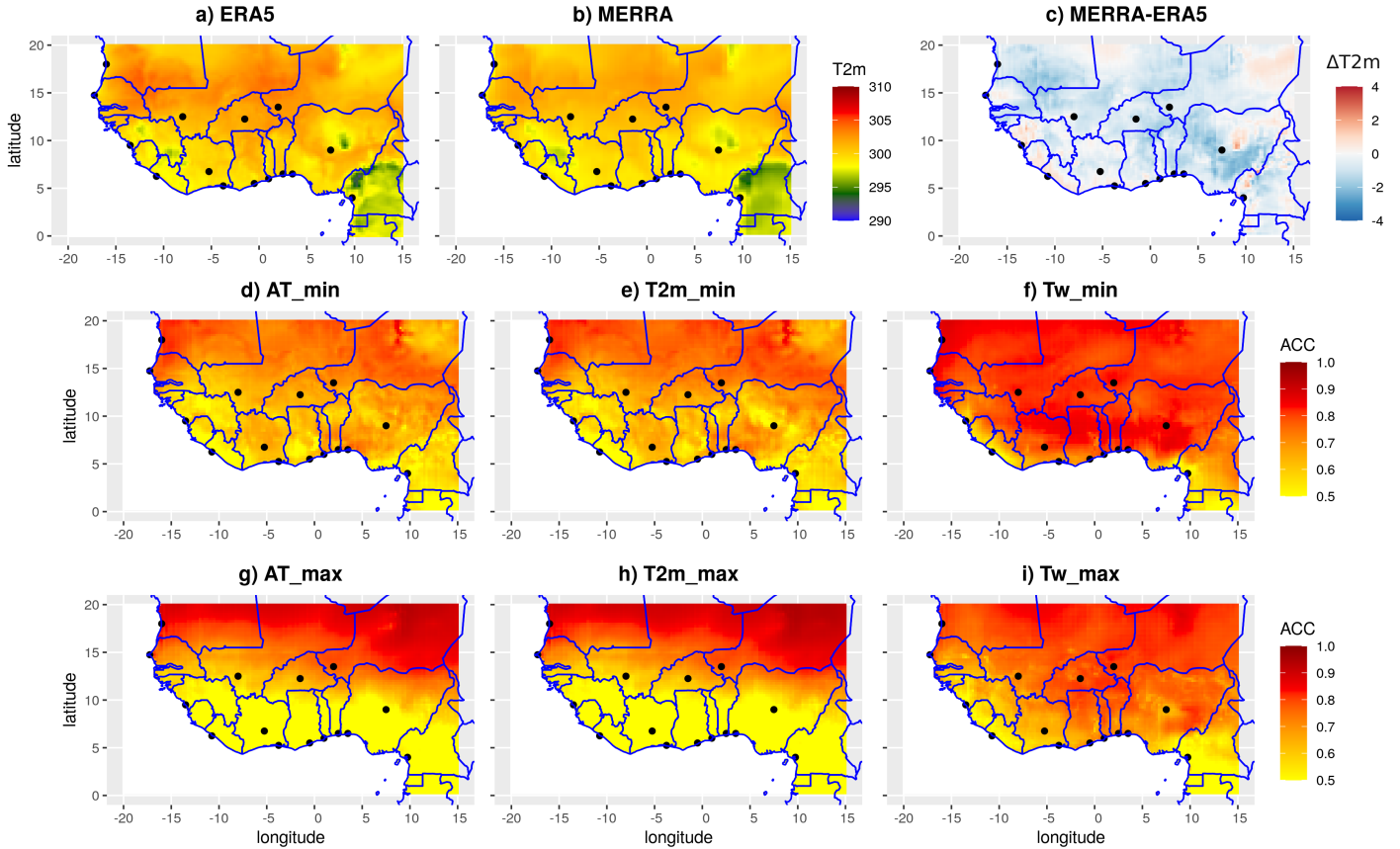
Figure 3. *Evaluation of products: a-b) Climatology state of T2m over 1993-2020 respectively for ERA5 and MERRA ; c) Climatological bias between MERRA and ERA5 using ERA5 as reference ($\Delta T2m$). d-f) / g-i) Anomaly of correlation between MERRA and ERA5 respectively for min / max values using AT, T2m and Tw variables. X- and Y -axis represent the longitude and latitude in degrees respectively. The color bars show the temperature (T2m) in degree Kelvin and the values of anomaly of temperature (ACC) respectively. The black points in the map represent the cities of interest analysed in this work (see section region of interest for more details), this apply for all the maps in the paper.*
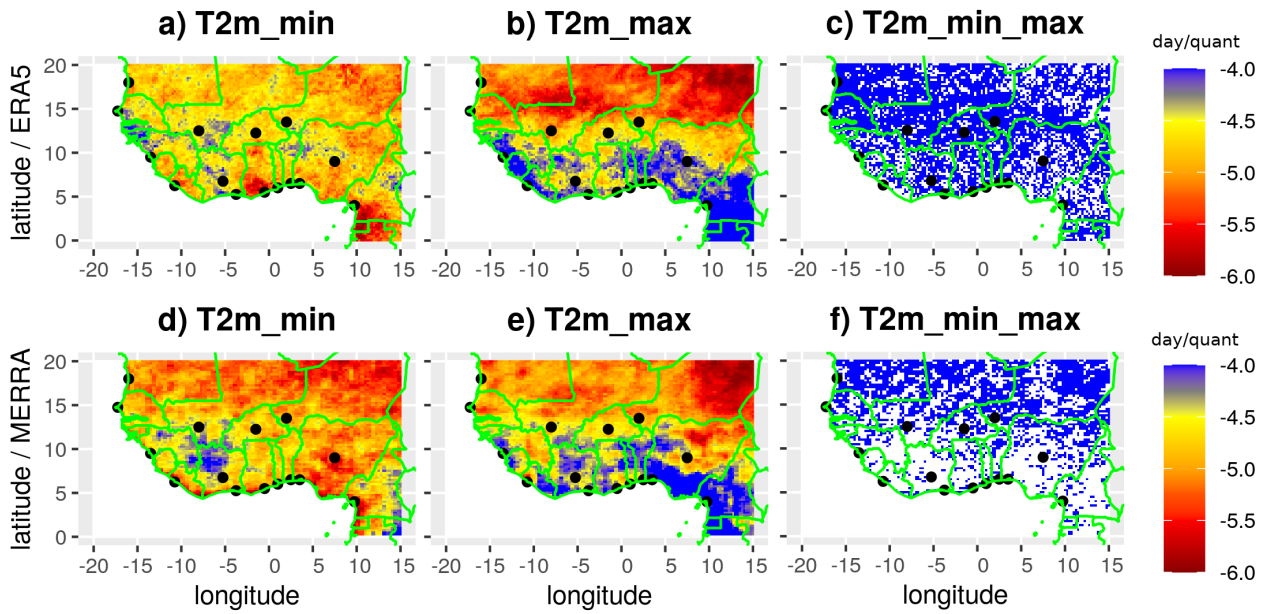
Figure 4. *Evolution of the heat wave duration with respect to the threshold values using T2m as indicator respectively for : a-c) ERA5 and d-f) MERRA. The slope of the regression line in day per percentile is computed by fitting a linear regression between the threshold values (Q75, Q80, Q85, Q90) and their corresponding heat waves's duration ($DQ_{75}, DQ_{80}, DQ_{85}, DQ_{90}$). X- and Y- axis represent the longitude and latitude in degrees respectively. The color bar shows the values of the slope. The white blanks indicate non significant changes in the duration of heat waves per percentile.The significance of the slope of the regression line has been computed using a two-sided Chi-square test.*
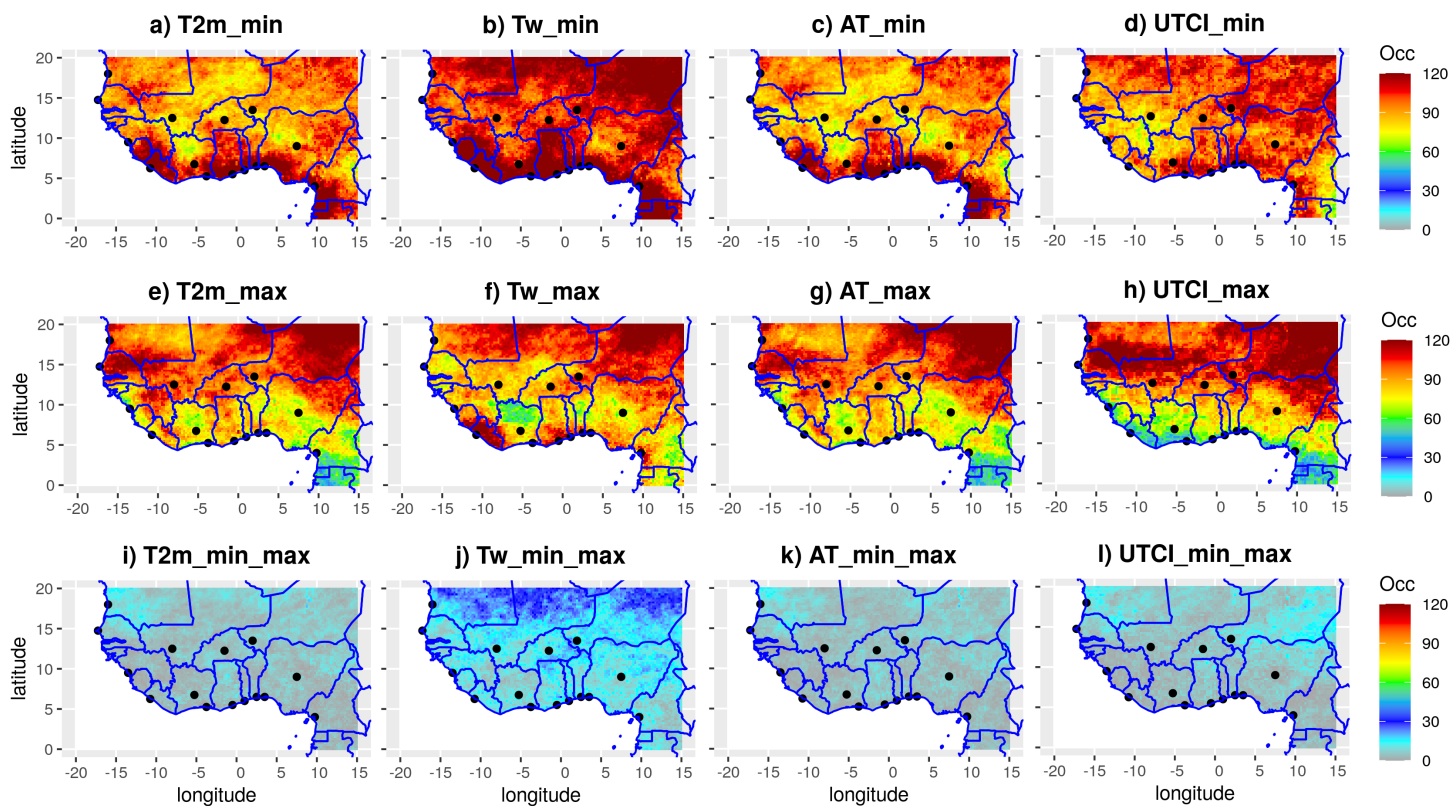
Figure 5. *Climatological state of heat wave occurrence over the period 1993-2020 using four different indicators for the heat wave detection ($T2m, Tw, AT, UTCI$) with respect to the definition of heat wave : a-d) minimum values of indicators, e-h) maximum values of indicators and i-l) minimum and maximum values of indicators. The detection of heat waves was processed using ERA5 reanalysis and the percentile 90th as a threshold. X- and Y- axis represent the longitude and latitude in degrees respectively. The color bar shows the frequency of events per region.*
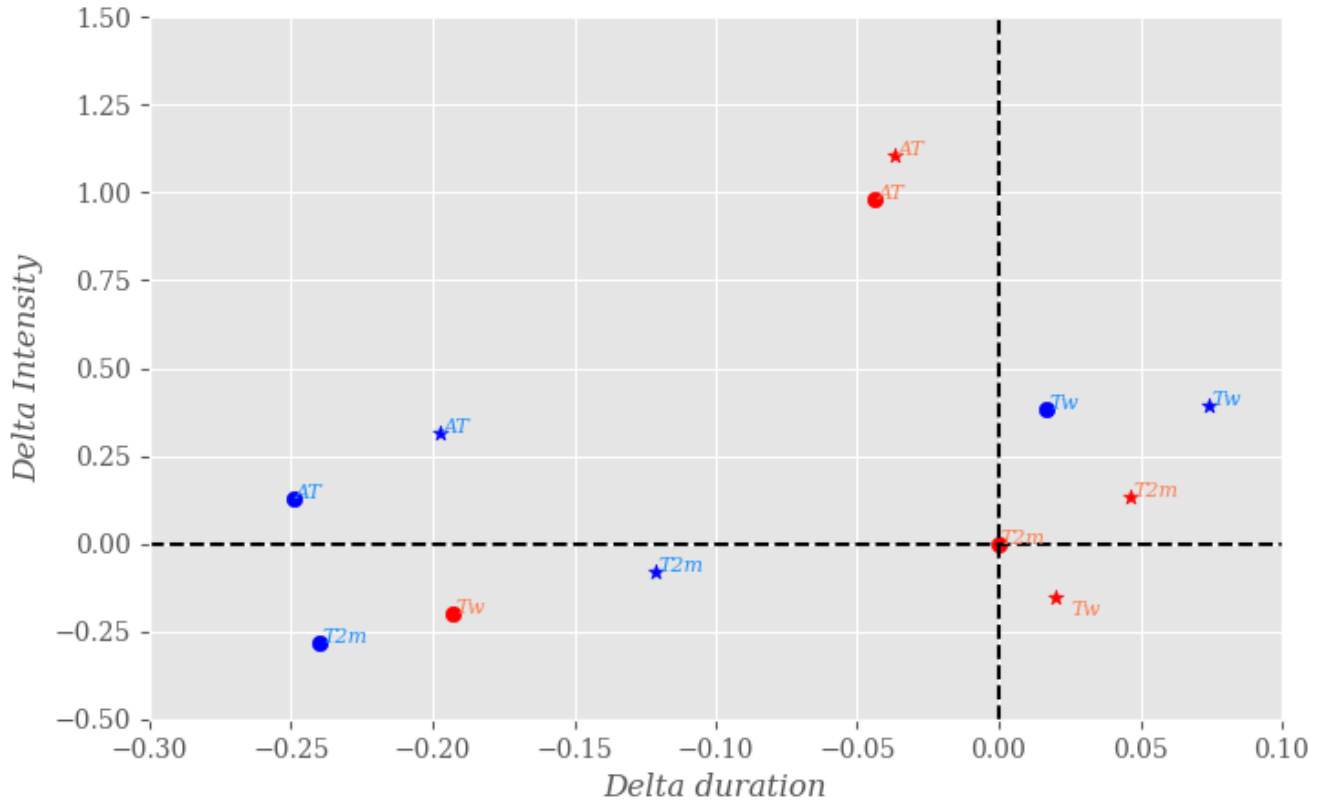
Figure 6. *Sensitivity of heat wave characteristics to the datasets, indicators and methodology used in the CONT region. The circles and stars in the figure represent respectively ERA5 and MERRA reanalyses. The blue/red color represents minimum/maximum values of the indicators. "$T2m_{max}$" from ERA5 is the reference variable used for the analysis. The Y- and X- axis show the standardized variation of intensity and duration respectively from the reference (no unit). The variation of duration and intensity have been computed using max daily T2m in ERA5 as reference. The detection of heat waves is done using the 90th as threshold.*
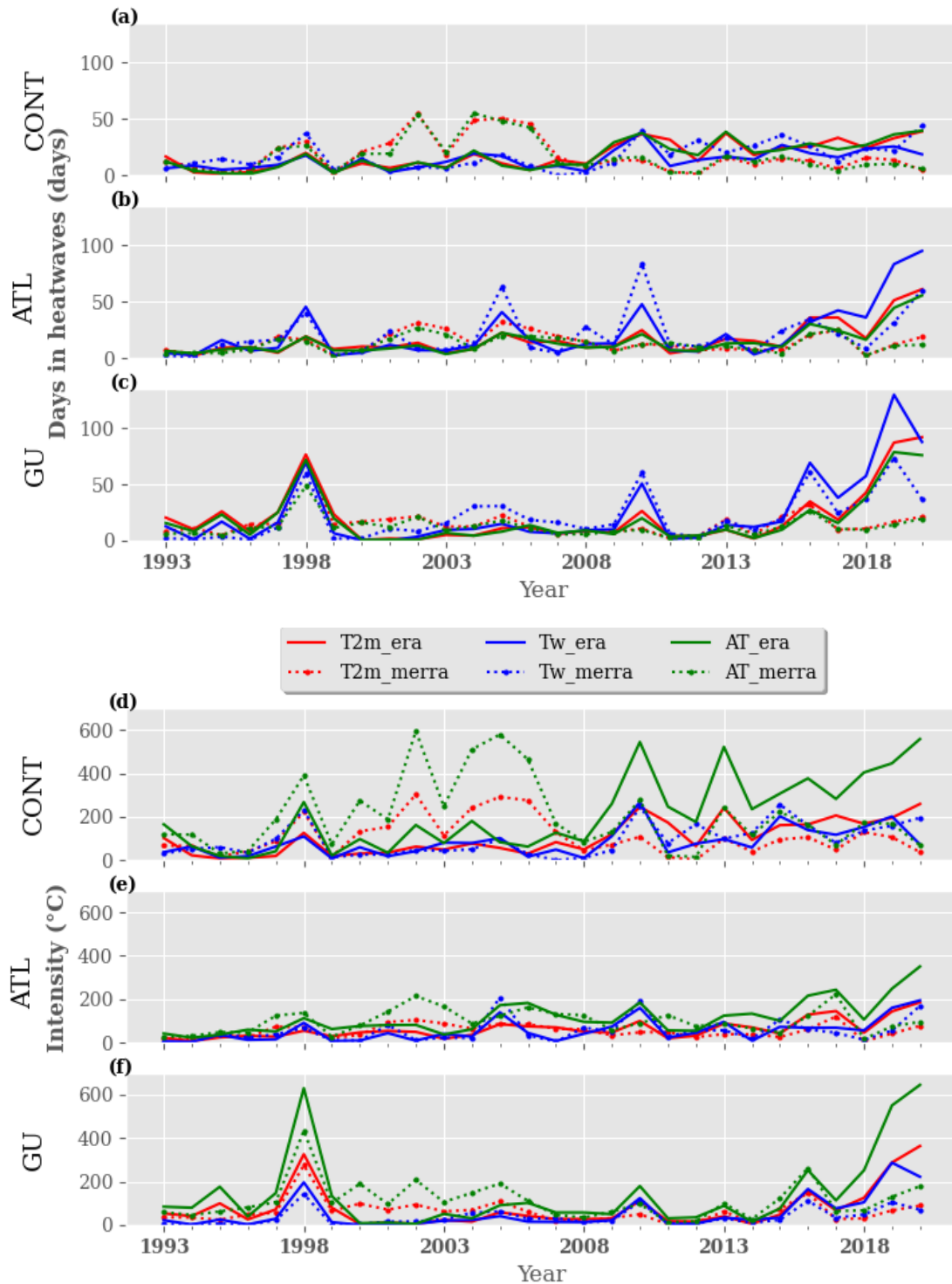
Figure 7. *Interannual variability of heat wave characteristics using maximum values of $T2m, Tw$ and AT : a-c) duration and d-f) intensity. The detection of heat waves is done using the 90th percentile as threshold over : a)$CONT$, b)ATL, c)GU regions. Red/blue/green strong and dashed lines represent the results using $T2m, Tw, AT$ from ERA5 and MERRA respectively. The Y- and X- axis represent the duration and intensity of heat waves and the time in year respectively.*
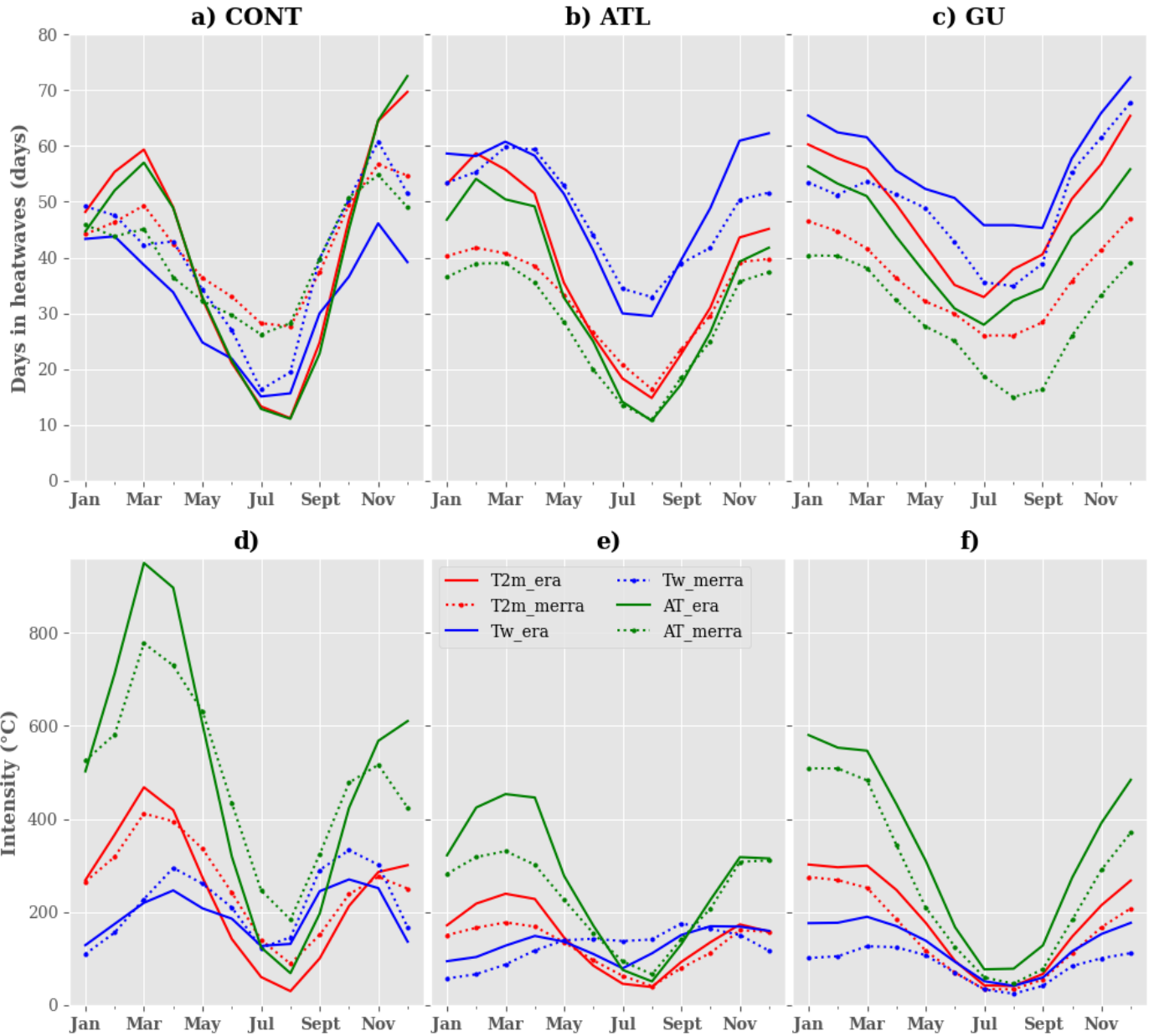
Figure 8. *Seasonal variability of heat waves characteristics using maximum values of $T2m, Tw, AT$: a-c) duration and d-f) intensity. We compute a 3-month running mean to smooth the seasonal cycle. The detection of heat waves is done using the 90th percentile as threshold over : CONT (a-d), ATL (b-e), GU (c-f) regions. Red/blue/green strong and dashed lines represent the results using $T2m, Tw, AT$ from ERA5 and MERRA respectively. The Y- and X- axis represent the duration and intensity of heat waves and the time in month respectively.*
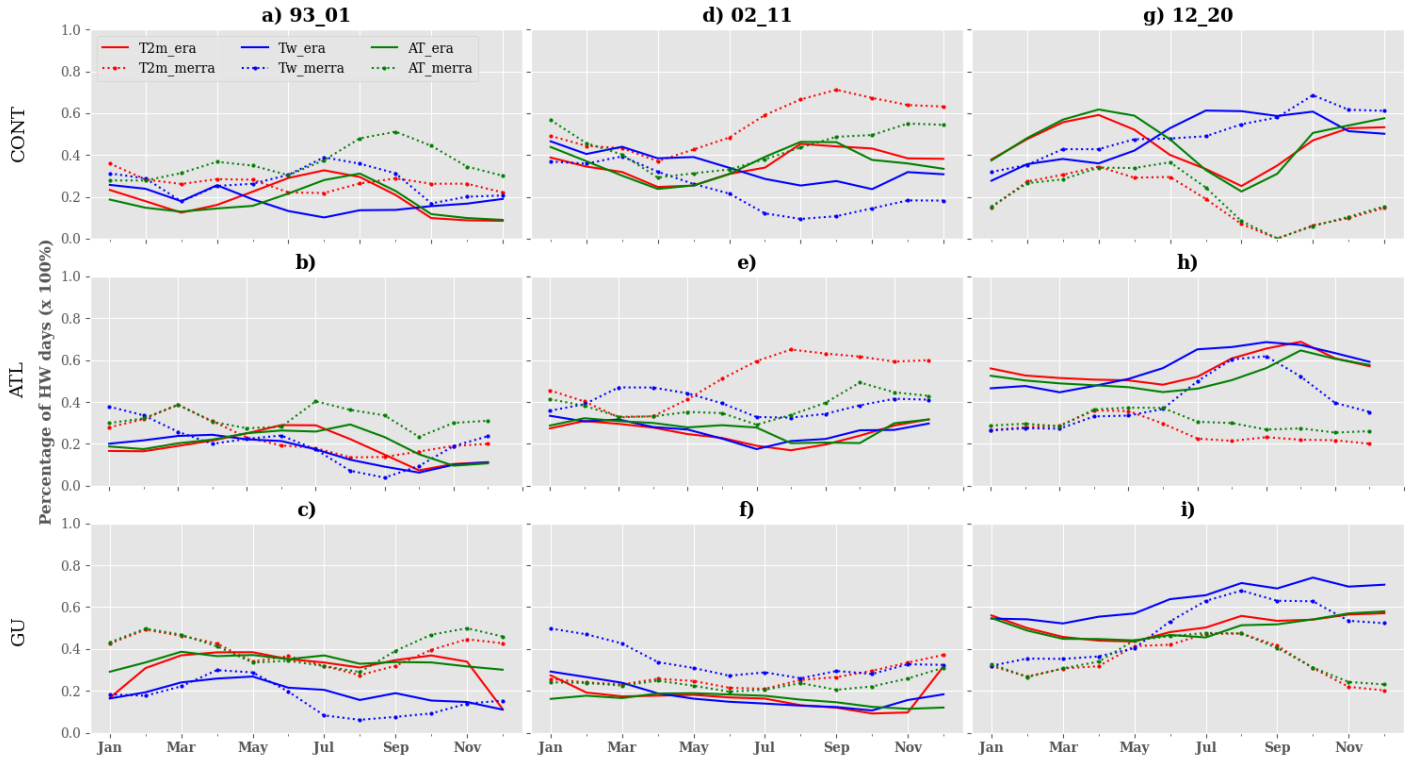
33

Figure 9. *Contribution in percentage of the different decades to heat wave duration using maximum values of $T2m, Tw, AT$ over the whole period respectively for : 1993-2001 (a-c), 2002-2011 (d-f) and 2012-2020 (g-i). We compute a 3-month running mean to smooth the seasonal cycle. The detection of heat waves is done using the 90th percentile as threshold over : CONT (a,d,g), ATL (b,e,h), GU (c,f,i) regions. Red/blue/green strong and dashed lines represent the results using $T2m, Tw, AT$ from ERA5 and MERRA respectively. The Y- and X- axis represent the percentage of heat wav days and the time in month respectively.*
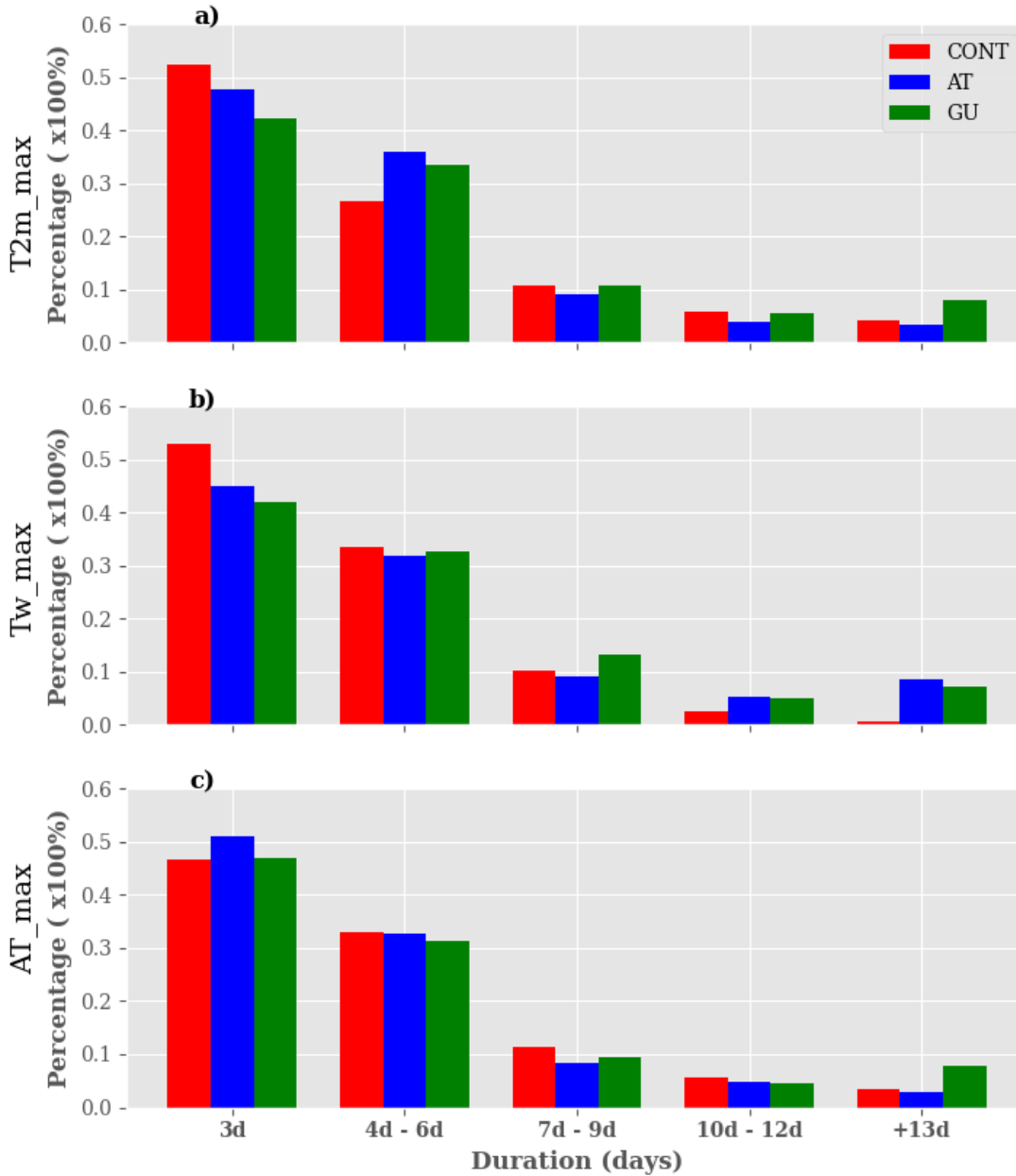
Figure 10. *Classification of heat waves detected with the 90th percentile as threshold using maximum values of indicators and ERA5 reanalysis based on their persistence over the period 1993-2020 : a) $T2m$, b) Tw and c) AT. Firstly, we detect heat waves and compute their duration; after we make some clusters of heat waves based on their duration (3d, 4d-6d, 7d-9d, 10d-12d, +13d) and finally, we quantify the proportion of each class of heat waves to the total number of events detected.* The Y- and X- axis represent the percentage of the heat waves per class and the duration in day respectively. Red/blue/green bars represent the percentage of heat waves detected over CONT/ATL/GU regions (see region of interest section for more details). The sum of the contribution of heat waves in different clusters is equal to 1 for each region.
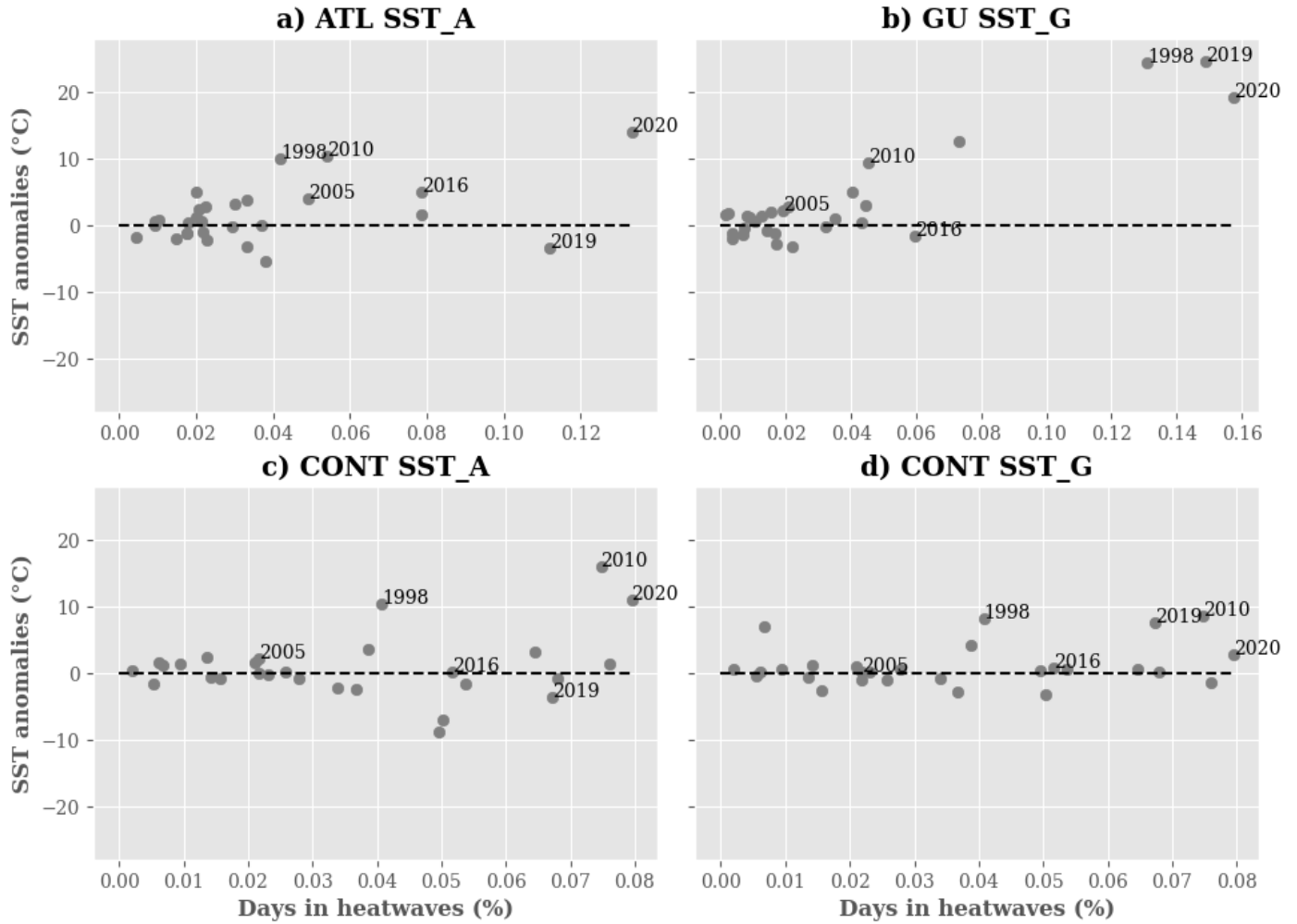
Figure 11. *Analysis of the link between SST anomalies and heat waves days over the period 1993-2020 using ERA5 reanalysis and maximum values of $T2m$: a)ATL, b)GU , $c-d$)CONT. The "SST_A" and "SST_G" represent boxes using to compute the SST mean anomalies for the ATL and CONT regions respectively (see [Fig1]). The anomalies are computed as the difference between monthly SST and the monthly climatological values of the SST over the whole period. For each year, the yearly anomalies of SST is computed with respect to the heat waves days. The X- and Y- axis represent the frequency of heat waves days and the SST anomalies respectively. The gray dots represent the years over the period 1993-2020.*